

EXPERIMENTAL AND NUMERICAL INVESTIGATION OF
A DIESEL AFTERTREATMENT SYSTEM

By

Andreato Maurizio

Dissertation Submitted to the Doctorate School
of the Politecnico di Torino in Partial Fulfillment of the
Requirements for the Degree of

DOCTOR OF PHILOSOPHY IN ENERGETICS
AT THE POLITECNICO DI TORINO



MAY 2015

Tutor:

Prof. Federico Millo

Scientific Committee:

Prof. Antonio Mittica

Prof. Fabio ORECCHINI

Prof. Francesco DI MARIA

“Considerate la vostra semenza:
fatti non foste a viver come bruti,
ma per seguir virtute e canoscenza”

Dante Alighieri

Aknowledgments

Abstract

Automotive diesel engines, thanks to their high efficiency, play a key role in the future global CO₂ emission reduction. However, the upcoming tighter regulations with the aim of reduction of the harmful pollutant emissions require the adoption of more complex after-treatment systems, where the integration between different components is mandatory in order to minimize the overall drawbacks and maximize the system efficiency. In particular, in this work a Diesel Particulate Filter (DPF) and a Diesel Oxidation Catalyst (DOC) were experimentally and numerically investigated, considering both the integration with other after-treatment components and the impact of the usage of different fuel compositions.

Since the properties of the filter substrate material play a fundamental role in determining the optimal soot loading level to be reached before DPF regeneration, three different filter substrate materials (Silicon Carbide, Aluminum Titanate and Cordierite) were investigated in this work, considering different driving conditions, after-treatment layouts and regeneration strategies.

In the first step of the research, an experimental investigation on the three different substrates over the New European Driving Cycle (NEDC) was performed. The data obtained from experiments were then used for the calibration and the validation of a one dimensional fluid-dynamic engine and after-treatment simulation model. Afterwards, the model was used to predict the vehicle fuel consumption increments as a function of the exhaust back pressure due to the soot loading for different driving cycles. The results showed that appreciable fuel consumption increments could be noticed only in particular driving conditions, and, as a consequence, in most of the cases the optimal filter regeneration strategy corresponds to the highest soot loading that still ensures the component safety even in case of uncontrolled regeneration events.

The diesel engine commercialization in emerging markets (like India and Asia) and the contemporary adoption of more stringent emission regulation set a further issue for the diesel after-treatment system performance, since the low diesel fuel quality enhances the risk of exceeding the emission limits. One of the most relevant characteristics of the low quality diesel fuel is the high sulfur content which has an adverse influence on emissions. Utilization of high sulfur fuel can cause deactivation of diesel catalyst and as a result higher amount of pollutants are observed at the tailpipe. For this reason it is crucial to

understand and mitigate sulfur impact and the extent of catalyst efficiency recovery through de-sulfation processes in order to increase the robustness of the EU5/6 diesel after-treatment systems also for markets with high sulfur fuel.

Considering the abovementioned issues, the impact of high sulfur fuel on the Diesel Particulate Filter and Diesel Oxidation Catalyst performance throughout different stages of New European Driving Cycle (NEDC) was experimentally tested on real size engine tests. In order to assess the impact of sulfur poisoning, a specific poisoning procedure was adopted which resulted in different sulfur poisoning levels. The impact of different space velocities on degreened, poisoned and de-sulfated system was examined and compared. In addition, the ability of recovering the performance of after-treatment system after regeneration through a proper de-sulfation strategy was evaluated with respect to fresh and degreened catalyst.

To come to the point, DOC showed a continuous loss of performance after each poisoning procedure, while DPF reached a steady state after a certain level of poisoning. DPF seemed to be capable of recovering the efficiency gap highlighted over the DOC only when lightly sulfur poisoned systems were considered. Moreover, light-off temperature was not affected by Space Velocity (SV) in the degreened catalyst, while for de-sulfated and poisoned catalyst the opposite was found. Besides, changing the SV revealed various impacts on the HC light-off curve.

List of abbreviations

ACEA	<i>European Automobile Manufactures Association</i>
ACT	<i>Asymmetric Cell Technology</i>
AFV	<i>Alternative Fuels Vehicles</i>
AT	<i>Aluminum Titanate</i>
BDC	<i>Bottom Dead Center</i>
CARB	<i>California Air Resources Board</i>
CD	<i>Cordierite</i>
CO	<i>Carbon Monoxide</i>
CO₂	<i>Carbon Dioxide</i>
CR	<i>Compression Ratio</i>
CPSI	<i>Cells per square inch</i>
CTE	<i>Coefficient of Thermal Expansion</i>
CVS	<i>Constant Volume Sampling</i>
DOC	<i>Diesel Oxidation Catalyst</i>
DPF	<i>Diesel Particulate Filter</i>
DeSOx	<i>Desulfatated Component</i>
DTI	<i>Drop To Idle</i>

ECU	<i>Engine Control Unit</i>
EGR	<i>Exhaust Gas Recirculation</i>
EPA	<i>Environment Protection Agency</i>
FC	<i>Fuel Consumption</i>
FRM	<i>Fast Running Model</i>
GHG	<i>Greenhouse Gases</i>
HAC	<i>Hexagonal Asymmetric Cell</i>
HEV	<i>Hybrid Electric Vehicles</i>
HC	<i>Unburned Hydrocarbons</i>
HCCI	<i>Homogeneous Charge Compression Ignition</i>
HCHO	<i>Formaldehyde</i>
HP	<i>High Pressure</i>
IMEP	<i>Indicated Mean Effective Pressure</i>
LD	<i>Light Duty</i>
LEV	<i>Low Emission Vehicle</i>
LNT	<i>Lean NO_x Trap</i>
LP	<i>Low Pressure</i>
LTC	<i>Low Temperature Combustion</i>
MIL	<i>Thousandth of inch</i>

MOR	<i>Modulus of Rupture</i>
MPG	<i>Miles per Gallon</i>
NA	<i>Not Available</i>
NEDC	<i>New European Driving Cycle</i>
NMHC	<i>Non-Methane Hydrocarbons</i>
NMOG	<i>Non-Methane Organic Gases</i>
NOx	<i>Nitrogen Oxide</i>
OEM	<i>Original Equipment Manufacturer</i>
OS	<i>Octagonal Square</i>
PCCI	<i>Premixed Charge Compression Ignition</i>
PM	<i>Particulate Matter</i>
PN	<i>Particle Number</i>
RCCI	<i>Reactivity Controlled Compression Ignition</i>
RGN	<i>DPF Regeneration</i>
S.C.	<i>Safety Coefficient</i>
SCR	<i>Selective Catalytic Reduction</i>
SFA	<i>Specific Filtration Area</i>
SiC	<i>Silicon Carbide</i>
SML	<i>Soot Mass Limit</i>

SOF	<i>Soluble Organic Fraction</i>
TFA	<i>Total Filtration Area</i>
SULEV	<i>Super Ultra Low Emission Vehicle</i>
ULEV	<i>Ultra Low Emission Vehicle</i>
WLTC	<i>Worldwide harmonized Light vehicles Test Cycle</i>

List of Figures

Figure I-1 Average fleet CO ₂ emissions in Europe [2].....	22
Figure I-2 Average CO ₂ emission targets for USA [3]	23
Figure II-1 Roller Bench Scheme.....	36
Figure II-2 a) Measured backpressure over the NEDC cycle at 0 g/l.....	38
Figure II-3 Exhaust temperatures at the DOC inlet and at the DPF outlet over NEDCs carried out with soot empty DPFs.....	38
Figure II-4 Thermocouples locations inside the DPF	40
Figure II-5 Temperature trends over the horizontal diameter of the rear DPF section (Thermocouples # 7 : 12 in Figure II-4) during a DTI event.....	40
Figure II-6 Temperature trends during regeneration events on a Silicon Carbide DPF at a soot loading of 10 g/l over NEDC (a) and drop to idle (b). The signals TC1, TC4, TC10 refer to the thermocouples # 1, 4, 10 shown in Figure II-4. The solid line labeled as Exh_tPFI.....	40
Figure II-7 Exhaust emission measurement layout [60]	42
Figure II-8 Light-off procedure, transient ramp cycle.....	46
Figure II-9- CO light-off curve obtained with the aid of transient ramp cycle	47
Figure III-1 Comparison between experimental and measured backpressure in the case of empty Cordierite component.....	49
Figure III-2 NEDC driving profile	50
Figure III-3 Artemis Urban driving profile	50
Figure III-4 Artemis Road driving profile.....	51
Figure III-5 WLTC driving profile	51
Figure III-6 Vehicle acceleration versus speed for the different driving cycles	51
Figure III-7 Simulation time comparison between different model types.	53
Figure III-8 Comparison between model average filter temperature, factored temperature and maximum substrate temperature measured in a DTI event.....	55

Figure III-9 Measured and weighted average DPF substrate temperature during a DTI event	55
Figure III-10 Comparison between model prediction and substrate Temperature in a Aluminum Titanate 11g/l DTI	56
Figure III-11 Comparison between model prediction and substrate Temperature in a Aluminum Titanate 06 g/l DTI	56
Figure III-12 Comparison between model prediction and substrate Temperature in a Silicon Carbide 08 g/l DTI.....	56
Figure III-13 Comparison between model prediction and substrate Temperature in a Silicon Carbide 11 g/l DTI.....	56
Figure III-14 Comparison between model prediction and substrate Temperature in a Silicon Carbide 13.5 g/l DTI.....	56
Figure III-15 Comparison between model prediction and substrate Temperature in a Cordierite 10 g/l DTI	56
Figure IV-1 Maximum temperature versus soot loading during the RGN event over the NEDC shown in Figure II-6a	59
Figure IV-2 Maximum temperature gradient versus soot loading during the RGN event over the NEDC shown in Figure II 6a	59
Figure IV-3 Maximum temperature versus soot loading during the DTI RGN event shown in Figure II 6b	59
Figure IV-4 Maximum temperature gradient versus soot loading during the DTI RGN event shown in Figure II 6b	59
Figure IV-5 Maximum temperature peak versus maximum temperature gradient reached during regenerations for Silicon Carbide.....	60
Figure IV-6 Maximum temperature peak versus maximum temperature gradient reached during regenerations for Cordierite	60
Figure IV-7 Maximum temperature peak versus maximum temperature gradient reached during regenerations for Aluminum Titanate	61
Figure IV-8 Regeneration efficiency as a function of maximum temperature (controlled RGN events during NEDC).....	62

Figure IV-9 Regeneration efficiency as a function of soot loading (controlled RGN events during NEDC)	62
Figure IV-10 Regeneration efficiency as a function of maximum temperature (uncontrolled RGN events during DTI).	62
Figure IV-11 Regeneration efficiency as a function of soot loading (uncontrolled RGN events during DTI).	62
Figure IV-12 Simulation of the Substrate Temperature in an AT DTI event with and without maximum temperature control strategy	64
Figure IV-13 Comparison between experimental data and model prediction in case of SiC DTI regeneration event.....	65
Figure IV-14 Comparison between experimental data and model prediction in case of AT DTI regeneration event.....	65
Figure IV-15 Comparison between experimental data and model prediction in case of Cd DTI regeneration event.....	65
Figure IV-16 Comparison between experimental data and model prediction in case of SiC regeneration over the NEDC cycle	65
Figure IV-17 Comparison between experimental data and model prediction in case of AT regeneration over the NEDC cycle	65
Figure IV-18 Comparison between experimental data and model prediction in case of Cd regeneration over the NEDC cycle	65
Figure IV-19 Number of NEDC cycles needed to load the component to trigger a regeneration normalized to Silicon Carbide (SML2 hypothesis) values.....	67
Figure IV-20 Number of Artemis Urban cycles needed to load the component to trigger a regeneration normalized to Silicon Carbide (SML2 hypothesis) values.....	67
Figure IV-21 Number of Artemis Road cycles needed to load the component to trigger a regeneration normalized to Silicon Carbide (SML2 hypothesis) values.....	68
Figure IV-22 Number of WLTC cycles needed to load the component so to trigger a regeneration normalized to Silicon Carbide (SML2 hypothesis) values.....	68
Figure IV-23 Influence of regeneration frequency on the oil life over the Artemis Urban ...	71

Figure V-1 NEDC global analysis for CO emissions for different poisoning levels; (a) CO abatement efficiency over DOC, (b) CO abatement efficiency over DOC+DPF	72
Figure V-2- NEDC breakdown analysis for CO emissions for different poisoning levels; (a) CO abatement efficiency over DOC, (b) CO abatement efficiency over DOC+DPF	73
Figure V-3- NEDC global analysis for HC emissions for different poisoning levels; (a) HC abatement efficiency over DOC, (b) HC abatement efficiency over DOC+DPF	73
Figure V-4- NEDC breakdown analysis for HC emissions for different poisoning levels; (a) HC abatement efficiency over DOC, (b) HC abatement efficiency over DOC+DPF	74
Figure V-5- Abatement efficiency over DOC and DOC+DPF as a function of poisoning level; (a) CO, (b) HC.....	74
Figure V-6-Temperature profile during NEDC for different poisoning levels; (a) downstream of DOC, (b) downstream of DPF	75
Figure V-7- NEDC global analysis for CO emissions for different de-sulfation levels; (a) CO abatement efficiency over DOC, (b) CO abatement efficiency over DOC+DPF	75
Figure V-8- NEDC global analysis for HC emissions for different de-sulfation levels; (a) HC abatement efficiency over DOC, (b) HC abatement efficiency over DOC+DPF	76
Figure V-9- Temperature profile during NEDC for different de-sulfation levels; (a) downstream of DOC, (b) downstream of DPF	76
Figure V-10- Light-off curve of degreened system for different space velocities; (a) CO, (b) HC.....	77
Figure V-11- Light-off curve of 3.58 gr/l sulfur (highly poisoned) system for different space velocities; (a) CO, (b) HC	77
Figure V-12- Light-off curve of DeSOx @ 3.58 gr/l system for different space velocities; (a) CO, (b) HC	78
Figure V-13 Light-Off temperature comparison degreened vs DeSOx	79

List of Tables

Table I.1 EU Emission Standards for Passenger Cars (source: Dieselnet, Emissions Standards - Europe - Cars and Light Trucks. 2011).....	19
Table I.2 Tier 2 Emission Standards (source: Dieselnet, Emissions Standards - USA - Cars and Light-Duty Trucks -Tier 2. 2011)	20
Table I.3 Emission Standards (source: TransportPolicy, Emission Standards - CARB - Cars and Light-Duty Trucks - Tier2. 2011).....	20
Table I.4 Emission Standards (source: Industry Insight, Emissions Standards - USA - Cars and Light-Duty Trucks -Tier 3, 2017-2025)	21
Table II.1 Engine Characteristics	31
Table II.2 Vehicle Technical Data	31
Table II.3 Materials properties (values* were not directly provided by the supplier but taken from literature [31]).	35
Table II.4 Delta fuel consumption, compared to SiC 0 g/l, over the NEDC cycle.....	38
Table II.5 After-treatment system characteristics	43
Table II.6 Elementary cycle for poisoning the aftertreatment system	44
Table II.7 Levels of sulfur poisoning	44
Table II.8 Operating points	45
Table III.1 Percentage Fuel Consumption increments as a function of backpressure	52
Table III.2 Percentage Fuel Consumption increment for the different WLTC Phases.....	52
Table IV.1 Fuel consumption increment compared to SiC for each soot mass limit hypothesis	70
Table IV.2 Fuel consumption reduction for each substrate respect the SML1 hypothesis.	70

Table of Contents:

Aknowledgments.....	3
Abstract.....	5
List of abbreviations	7
List of Figures	11
List of Tables.....	15
Table of Contents:	16
CHAPTER I. DIESEL EMISSIONS CONTROL TECHNOLOGIES REVIEW	18
I.1. Introduction.....	18
I.2. Regulatory developments.....	18
I.3. Engine Development	23
I.4. AFTER-TREATMENT TECNOLOGY DEVELOPMENT.....	25
I.4.1. Diesel Oxidation Catalyst (DOC).....	26
I.4.2. Diesel Particulate Filter (DPF)	27
I.4.3. Nitrogen Oxides After-Treatment technologies.....	28
CHAPTER II. EXPERIMENTAL APPARATUS AND TEST PROCEDURES	30
II.1. Introduction.....	30
II.2. DPF Substrate investigation.....	30
II.2.1. Engine and Vehicle Characteristics	30
II.2.2. Tested Substrate Materials.....	31
II.2.3. Experimental Set-Up and Test Procedure	35
II.3. DOC Sulphur Poisoning Investigation	42
II.3.1. Experimental Set-up	42
II.3.2. Test Procedure.....	44
CHAPTER III. ENGINE AND DPF MODEL SET UP	48
III.1. INTRODUCTION	48
III.2. 1D ENGINE MODEL SET-UP.....	48
III.3. DPF MODEL SET UP.....	52
CHAPTER IV. SOOT MASS LIMIT IMPACT ON FUEL CONSUMPTION AND OIL DILUTION	57
IV.1. INTRODUCTION	57
IV.2. EXPERIMENTAL RESULTS: SOOT MASS LIMIT TESTS	57
IV.3. DPF REGENERATION MODEL RESULTS.....	63

IV.4. SOOT MASS LIMIT IMPACT ON FUEL CONSUMPTION AND OIL DILUTION	66
CHAPTER V. ANALYSIS OF SULPHUR POISONING EFFECT ON DOC CONVERSION EFFICIENCY	72
V.1. INTRODUCTION	72
V.2. CC(DOC+DPF) PERFORMANCE CHARACTERIZATION.....	72
V.2.1. Degreened vs. poisoned	72
V.2.2. Recovery of efficiency after de-sulfation compared to degreened.....	75
V.3. CC(DOC+DPF) LIGHT-OFF CURVES	76
Conclusions	80
Bibliography:	82
List of Publications	92

CHAPTER I. DIESEL EMISSIONS CONTROL TECHNOLOGIES REVIEW

I.1. Introduction

Since the object of this work is an experimental and numerical investigation of a diesel after-treatment system, whose main purpose is the abatement of tail pipe pollutants emissions, a short overview of the main regulations trends and after-treatment technologies will be given in this chapter.

I.2. Regulatory developments

In the last years the legislation limits in terms of pollutants limits for LD vehicles are becoming always more stringent, forcing all the OEMs to improve engine and after-treatment technologies in order to match the required emission limits. For this reason a short description about the emission legislation evolution over the last decades will be provided hereafter; it is also worth to note that the following description will be focused only on LD diesel engines emission regulation, since gasoline engines are not considered in this work. Emission regulations in European countries for LD applications were first introduced in the '70 with Directive 70/220/EEC which, across the years, has been amended several times up to 2004, while in 2007 this Directive has been repealed and replaced by Regulation 715/2007 (usually referred to as Euro 5/6). Some of the important regulatory steps implementing emission standards for Diesel engines for LD vehicles are summarized in Table I.1. Tail pipe emissions limits, which are evaluated over the cold start cycle referred as NEDC (New European Driving Cycle), were progressively reduced from EU1 up to the current EU6 legislation. Starting from EU4, the legislation tightening was mainly focused on NO_x and PM emissions, in particular, after the introduction of EU5b, a limit on particulate number (PN) was also introduced in addition to the limit on particulate mass (PM). Setting the limitations only on PM may lead to the emission of smaller and lighter soot particles which are extremely dangerous for the human health and environment, hence PN limits are added to avoid this issue [1]

Stage	Date	g/km					PN #/km
		CO	HC	HC+NOx	NOx	PM	
Euro 1	1992 - 07	2,7	-	0,97	-	0,140	
Euro2, IDI	1996 - 01	1,0	-	0,70	-	0,080	
Euro 2, DI	1996 - 01	1,0	-	0,90	-	0,100	
Euro 3	2000 - 01	0,6	-	0,56	0,50	0,050	
Euro 4	2005 - 01	0,5	-	0,30	0,25	0,025	
Euro 5a	2009 - 09	0,5	-	0,23	0,18	0,005	
Euro 5b	2011 - 09	0,5	-	0,23	0,18	0,005	6×10^{11}
Euro 6	2014 - 09	0,5	-	0,17	0,08	0,005	6×10^{11}

Table I.1 EU Emission Standards for Passenger Cars (source: Dieselnet, Emissions Standards - Europe - Cars and Light Trucks. 2011)

The USA emission standards differ significantly from the EU ones since they are fuel neutral, meaning that the same targets have to be achieved both from gasoline and diesel engines; Federal Standards for engines and vehicles, including emission standards for greenhouse gas (GHG) emissions, are established by the US Environmental Protection Agency (EPA).

Two categories of standards have been defined for LD vehicles in 1990; Tier 1 standards, published as a final rule on June 5, 1991 and phased-in progressively between 1994 and 1997 and Tier 2 standards, adopted on December 21, 1999, with a phase-in implementation schedule from 2004 to 2009. The introduction of Tier 2 standards imposed a more stringent numerical emission limits with respect to the previous Tier 1 requirements, and a number of additional changes that made the standards more stringent for larger vehicles. Under the Tier 2 regulation, the same emission standards are applied to all vehicle weight categories (i.e. cars, minivans, light-duty trucks, and SUVs have the same emission limit). Table I.2 reports the Tier 2 emission standards that are structured in 8 different permanent levels, named as “*certification bins*”. Each car manufacturer may choose to certificate particular vehicles in one of the different bins, but with the clause that the average NOx emission of the LD vehicles fleet, for each manufacturer, has to meet the Tier II Bin#5 emission standards. The three temporary bins reported in Table I.2 were used during the phase-in period and are not valid any more since the model year 2008.

Bin	Date	CO	NMHC	HCHO	NOx	PM
		g/mi				
Temporary Bins						
11	2004-2008	7,3	0,280	0,032	0,90	0,12
10	2004-2008	4,2	0,156	0,018	0,60	0,08
9	2004-2008	4,2	0,090	0,018	0,30	0,06
Permanent Bins						
8	2008-2017	4,2	0,125	0,018	0,20	0,02
7	2008-2017	4,2	0,090	0,018	0,15	0,02
6	2008-2017	4,2	0,090	0,018	0,10	0,01
5	2008-2017	4,2	0,090	0,018	0,07	0,01
4	2008-2017	2,1	0,070	0,011	0,04	0,01
3	2008-2017	2,1	0,055	0,011	0,03	0,01
2	2008-2017	2,1	0,010	0,004	0,02	0,01
1	2008-2017	0,000	0,000	0,000	0,000	0,000

Table I.2 Tier 2 Emission Standards (source: Dieselnet, Emissions Standards - USA - Cars and Light-Duty Trucks -Tier 2. 2011)

In addition to the Federal standard, the State of California, through its California Air Resources Board (CARB) authority, has the right to develop its own emission standards (Table I.3). Similarly to the federal limits also the Californian ones are organized in different bins: Low Emission Vehicles (LEV), Ultra Low Emission Vehicles (ULEV) and Super Ultra Low Emission Vehicles (SULEV). As in the federal legislation, individual vehicle models can be certified in specific bins, with the clause to meet, with manufacturer's fleet average emissions, a designated average for tailpipe. The CARB certification requirements are usually more severe than the EPA ones, thus requiring a major effort in terms of engine and after-treatment development.

Bin	Date	CO	NMHC	HCHO	NOx	PM
		g/mi				
50000 miles/5 years						
LEV	2004-2017	3,4	0,075	0,015	0,05	-
ULEV	2004-2017	1,7	0,04	0,008	0,05	-
SULEV	2004-2017	-	-	-	-	-
120000 miles/11 years						
LEV	2004-2017	4,2	0,075	0,018	0,070	-
ULEV	2004-2017	2,1	0,040	0,011	0,070	-
SULEV	2004-2017	1,0	0,000	0,004	0,020	-

Table I.3 Emission Standards (source: TransportPolicy, Emission Standards - CARB - Cars and Light-Duty Trucks - Tier2. 2011)

The Level III emissions standards, reported in Table I.4, will be phased in through model years 2017-2025. The new federal limits will be closely aligned to the Californian’s Level III standards and will maintain a similar structure in different bins, with the requirement, for each manufacturer, to meet a defined fleet average emission in a given model year. The new limits will require another significant reduction of the fleet average pollutants emissions with an increased requirement in terms of after-treatment system durability up to 120000 miles for EPA and up to 150000 for CARB homologation.

Bin	Date	CO	NMHC + NOx	HCHO	PM
		g/mi			
Permanent Bins					
160	2017-2025	4,2	0,160	0,004	0,003
125	2017-2025	2,1	0,125	0,004	0,003
70	2017-2025	1,7	0,070	0,004	0,003
50	2017-2025	1,7	0,050	0,004	0,003
30	2017-2025	1,0	0,030	0,004	0,003
20	2017-2025	1,0	0,020	0,004	0,003
0	2017-2025	0,000	0,000	0,000	0,000

Table I.4 Emission Standards (source: Industry Insight, Emissions Standards - USA - Cars and Light-Duty Trucks -Tier 3, 2017-2025)

From a general point of view, looking at the increasing tightening of emission limits for both the European and the American standards, it is possible to observe that the trend is to force the adoption of emission controlling technologies, whether they are in-cylinder or after-treatment, which could significantly bring down tailpipe emissions from mobile sources. Moreover the increasing mileage required for emission compliance will require additional efforts in order to reduce the aging effect on the overall system performance. A more detailed discussion about such technologies will be given in paragraphs I.3 and I.4.

Besides the reduction of pollutant emissions described so far, vehicles fuel economy has gained a lot of attention through years, becoming today a worldwide important topic of discussion; not only pollutant emissions have to be controlled, but also fuel consumption should be kept within regulated limits, which somehow highlights the global efforts to increase as much as possible the internal combustion engine efficiency and to reduce the emission of CO₂, which is the best known greenhouse gas (GHG). In order to reduce the CO₂ emissions, the European Commission signed 1998-99 a voluntary agreement with the European Automobile Manufacturers Association (ACEA) to reach a 25% CO₂ emissions

reduction, compared to the 1995 levels, by 2008. Even if a significant CO₂ reduction was achieved in the first years, the ACEA was not able to reach the 140 g/km. Then, the European Commission decided in 2009 to turn the voluntary agreement into a mandatory CO₂ emission regulation from new LD vehicles. The new limits imposed from the European Commission require an average CO₂ emission of 95 g/km as long term target, for each manufacturer's sold vehicle fleet. Besides incentives obtained respecting the targets, significant penalties will be applied to manufacturers which will not fulfill the limits; after a period (2012-2018) of progressively increasing fees, starting from 2019 manufacturers will pay €95 per vehicle for each g/km of CO₂ exceeding the target.

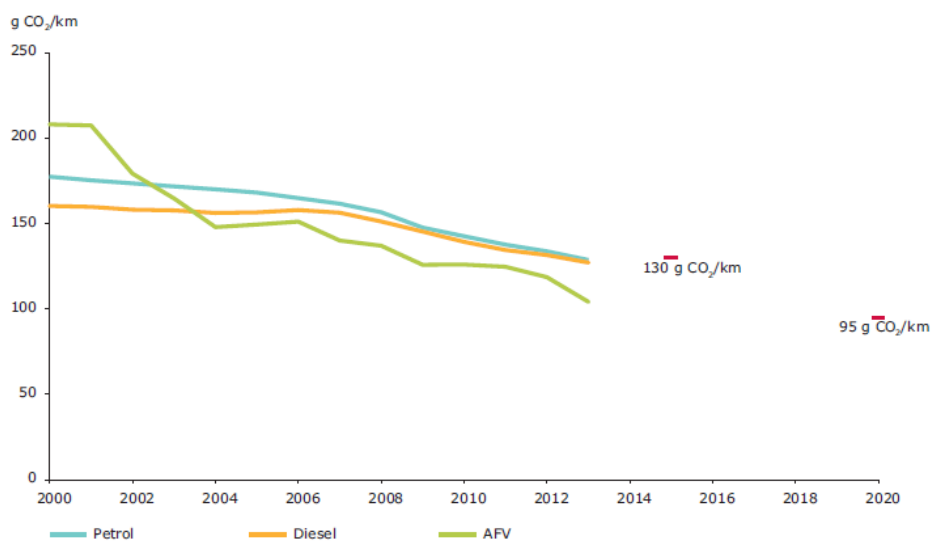


Figure I-1 Average fleet CO₂ emissions in Europe [2]

In USA the Corporate Average Fuel Economy (CAFE) standards for passenger cars and light duty trucks (LDT) was first established back in 1975 as part of the Energy Policy Conservation Act promoted as a response to the oil crisis of the early '70; the CAFE regulation requires each car manufacturer to meet a standard for the sales-weighted fuel economy, expressed in miles per gallon (mpg), for the entire fleet of vehicles sold in the USA in each model year. Figure I-2 shows the decreasing trend for CO₂ emissions imposed by EPA and CARB; by 2025 a fleet-wide level of 163 g/mi has to be achieved, corresponding to an average fuel consumption of 54.5 miles per gallon (mpg).

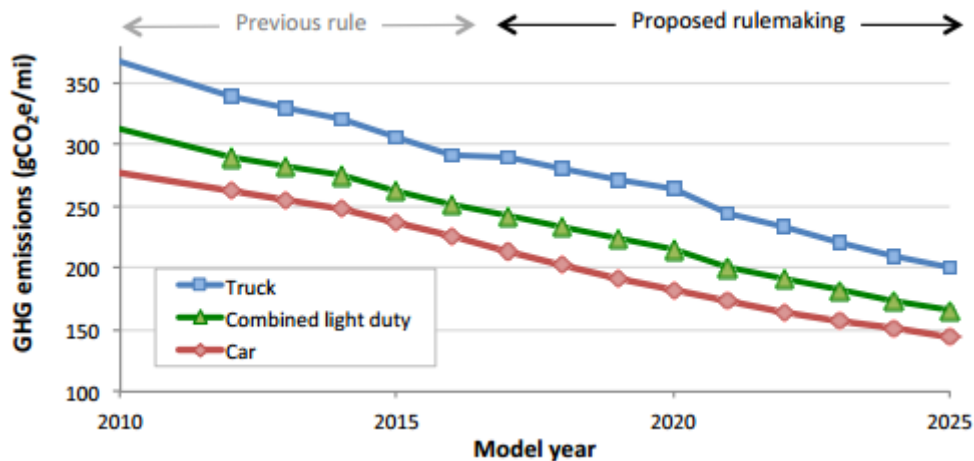


Figure I-2 Average CO₂ emission targets for USA [3]

I.3. Engine Development

Progresses in emissions regulations (*i.e.* from emerging SULEV standards in California), evolution of the market and upcoming fuel economy requirements are making great pressure on the Diesel engine, especially if considering the continuous evolution of advanced gasoline concepts and hybrid electric vehicles (HEV). Diesel engine developers are responding to the challenge focusing on the reduction of fuel consumption while maintaining good performance; this is mainly achieved through the adoption of very sophisticated combustion designs and control on the engine. Thanks to advances in turbocharging and fuel injection technologies, engine downsizing is today a very effective method to bring down engine fuel consumption without sacrificing engine performance; exhaust gas recirculation (EGR) control, two-stage turbocharging, closed-loop combustion control, advanced swirl concepts realized through variable valve actuation are other key technologies for the achievement of further improvements [4].

It is worth to note that the achievement of the future emission levels can be attained only through a synergic combination of different technologies involving both engine and after-treatment technologies developments. As a matter of fact, the last generation of diesel engines will adopt two stage turbocharging, high and low pressure EGR, high pressure injection systems (up to 2500bar) and an integrated after-treatment designed to reach a fast warm-up ensuring low tail-pipe emissions [5], [6].

From a more scientific point of view, downsized prototype diesel engines are reaching very high levels of specific power and Indicated Mean Effective Pressure (IMEP) [7]; however, even though downsizing and downspeeding of the engine can give undoubted benefits in terms of fuel consumption, an increase up to 50% in engine-out NO_x could be reached. On production engines, downsizing enables great savings in fuel consumption, but appropriate measures should be taken in order to compensate for the unavoidable increase of engine-out NO_x. One of the most adopted solutions, in order to decrease engine out NO_x emissions, is the addition of a low pressure EGR (LP EGR) system to the high pressure one. As a matter of fact, several studies [8], [9], [10] [11] showed that mixing colder exhaust gases to the intake air before the turbocharger, allows a better NO_x – Soot trade-off leading to remarkable benefits in terms of emission reduction without fuel consumption drawbacks. Another key component for the engine performance improvement is the injection system: as shown in [12], [13] the adoption of piezoelectric injectors will allow to raise the rail pressure up to 3000 bar. To bring the pilot injections closer to each other with an extreme accuracy in the injected quantity control for each injection. Thanks to these new injection patterns and advanced injection quantity control, remarkable reductions in terms of pollutants emissions and fuel consumption can be achieved.

As far as compression ratio (CR) is concerned, decreasing the diesel engine CR could lead to a reduction of frictional losses and NO_x, as reported by [14]; however lower compression ratios compromise thermodynamic efficiency and could result in poor cold start, especially in cold ambient conditions or at high altitude. The issue could be addressed by redesigning the bowl, adding more holes to the injector to get more air entrainment, and increasing the number of pilot injections [15]. More recently, in order to overcome these limitations, the adoption of a variable valve lifting also for diesel engines was investigated. The anticipation of the exhaust valve closure at low engine speed, gives the possibility to increase the effective compression ratio, thus achieving a higher gas temperature and pressure at the end of the compression phase..

On the other hand, advance combustion regimes have been widely investigated, with the aim to reduce emission of NO_x and PM which are more critical for diesel engines; Low Temperature Combustion (LTC) modes, which cover a number of advanced combustion strategies, including Homogeneous Charge Compression Ignition (HCCI), Premixed Charge Compression Ignition (PCCI) or Reactivity Controlled Compression Ignition

(RCCI), seem to be very promising in this context, but often present as a drawback an increase in CO and HC emissions. The NO_x emissions decrease can be achieved thanks to the significant reduction of thermal NO formation process due to lower combustion temperature, in the same way also PM emissions decrease thanks to significantly lower soot formation rate resulting from the combustion temperature lowering [16]. Conversely, higher CO emissions can result from under-mixed fuel-rich regions at high loads, or due to over-mixed fuel-lean regions at low loads [17] and from a slower oxidation of CO to CO₂ due to lower combustion temperature [18]. HC emissions can increase due to several factors such as long spray penetration, which leads to wall impingement, lowers combustion peak temperature at low loads, which causes quenching at combustion chamber surfaces, and a significant amount of fuel in lean zones that prone to escaping the burning process. In order to reduce these drawbacks, recent studies [19], [20] have investigated the use of oxygenated fuels (as Biodiesel) or the use of different blends of gasoline and diesel [21].

In addition to pollutant emissions, it should be also taken into account that in premixed LTC combustion, the combustion rate is not directly linked to the injection rate, which means that combustion cannot be controlled by the injection rate. As the name suggests, advanced combustion regimes are characterized by a more intense premixed portion of the combustion, whose main drawback is an increased combustion noise. In conventional diesel engines combustion noise was decreased significantly thanks to the advent of common rail injection systems that allowed the use of pilot injections in order to reduce the pressure gradient associated with premixed burning. For these reasons LTC modes can be operated nowadays only under low load engine operating conditions, through a synergic exploitation of the flexibility given by the common rail injection system and advanced EGR and turbocharger technologies, while still keeping a more conventional combustion regime under medium-high loads operating conditions.

I.4. AFTER-TREATMENT TECHNOLOGY DEVELOPMENT

In the following paragraphs, developments in after-treatment technologies, in particular for DOCs, DPFs and NO_x after-treatment systems, carried out in recent years will be presented; for the sake of brevity, fundamentals concerning operating principles of each after-treatment technology will not be discussed and will be taken for granted. However,

details about fundamentals for each of the following after-treatment devices are well described and summarized in [22].

I.4.1. Diesel Oxidation Catalyst (DOC)

The Diesel Oxidation Catalyst was the first after-treatment component introduced at the beginning of the 90s. Its main purpose is oxidizing CO and HC by oxygen availability in the diesel exhaust gas stream, however, in the recent years, this component gained a lot of importance, since it has also a non-trivial impact on the performances of the other after-treatment systems like DPF and SCR.

As a matter of fact besides the oxidation of CO and HC, DOC can convert great part of the soot SOF (Soluble Organic Fraction) thus reducing the total particulate mass at the DPF inlet, moreover the DOC capability of oxidizing HCs, is used during the active DPF regeneration phases to raise the exhaust temperature up to 600 °C. In addition, DOC can be specifically formulated, using Pt and Pd as precious metals, in order to promote the oxidation of NO into NO₂ [23], which even though is always a pollutant, plays a key role in the SCR conversion efficiency increase and in the passive soot oxidation inside the DPF. However, as shown in [24] and [25], as long as the light off temperature for CO and HC oxidation reactions is reached, the NO₂ conversion is reduced and NO₂ is consumed. A further issue is related to the HC slip over the DOC, in particular, as reported in [26], the HC slip may affect the NO₂ conversion over a catalyzed DPF. These phenomena give even more importance considering the increase of the light off temperature for CO and HC oxidation, related to the component aging [27], [28], and the additional drawbacks in terms of reduced NO_x conversion efficiency if a downstream SCR system were adopted.

In particular in extra European Markets, like India and South America, a further issue that has to be taken in account consists of the high sulfur content in diesel fuel. As a matter of fact the Sulphur, contained in diesel fuel, not only generates harmful SO_x emissions as combustion product, but also enhances the risk of the catalytic sites deactivations. In fact SO_x tends to bound permanently to the catalytic sites leading to their deactivation. In this case, the original component efficiency can be restored raising the exhaust temperature up to 600 °C and ensuring a rich exhaust mixture. However this process, similar to the DPF regeneration, has as main draw-back an increased fuel consumption and oil dilution.

I.4.2. Diesel Particulate Filter (DPF)

Since 2009 wall flow Diesel Particulate Filters (DPFs) have been adopted for all European passenger cars, in order to comply with the Particulate Matter (PM) EU5 emission limits.

Several studies [29], [30], [31], [32], [33] showed how DPFs are capable of physically capturing diesel particulates with extremely high filtration efficiencies, thus preventing their release into the atmosphere. However, the accumulation of the solid fraction of particulate matter over the filter, which is mostly represented by elemental carbon or soot, would eventually lead to the build-up of excessively high back pressures at the engine exhaust, if the accumulated particles were not removed, by means of the so called filter regeneration process, which basically consists of the oxidation of soot.

As well as DOC, DPF performances may have significant impacts on the overall engine and after-treatment efficiency. In addition to the key role in the particulate mass filtering described above, DPF presents a catalysed washcoat, that during the regeneration process decreases the activation energy of the soot oxidation, while during the normal engine operation leads to the conversion of NO into NO₂ thus increasing the SCR conversion efficiency. DPF properties may also influence the SCR warm-up phases, as a matter of fact a lower DPF thermal mass leads to a lower exhaust temperature loss through the component thus resulting in hotter gases at the SCR inlet. On the other hand, a lower thermal mass may result in a component cracking during critical regeneration phases and, consequently, in a permanent filtration efficiency loss [34]. This, in addition to the risk of not compliance with the emission standards, may also have negative impacts on the overall engine efficiency if a long route EGR system is adopted.

Finally DPF influences also the engine fuel consumption, in fact, as reported in [32] the optimal regeneration soot loading has to be chosen in the trade-off between the fuel consumption savings, related to a lower regeneration frequency, and the fuel consumption drawbacks related to the increased filter backpressure.

In order to harmonize the above described requirements, the research on DPF is focused on one side on the substrate materials and on the other side on the calibration strategies. The research on the substrate material aims to obtain filters with a higher thermal shock resistance [35] and filtration efficiency [36], but at the same time, with lower backpressure and thermal mass. On the other side, the improvements in the injection and calibration

strategies may reduce the fuel consumption and oil dilution drawbacks related to the active filter regeneration.

I.4.3. Nitrogen Oxides After-Treatment technologies

As discussed in the paragraph I.2, the future regulatory developments will call for the adoption of specific after-treatment strategies, since it will be no more possible to achieve the tailpipe NO_x emission targets only through combustion control techniques, Even if the pressure and temperature conditions are favourable for the NO_x reduction to N₂, the lean environment, that characterizes the diesel exhaust gases, makes the NO_x spontaneous reduction rate near to 0. As a consequence, the adoption of specific after-treatment components is necessary in order to enhance this reaction through a catalyst. The two actual leading technologies for the after-treatment NO_x reduction are the:

- SCR (Selective Catalytic Reduction): This system is usually placed downstream the DPF, and provides a continuous NO_x reduction through the injection of NH₃.
- LNT (Lean NO_x Trap): This component absorbs in specific catalytic sites the NO_x molecules and then promotes their reduction when a rich mixture is reached.

The SCR, once reached its light off temperature (about 200°C), presents NO_x conversion efficiencies above 90%; however, since it is usually placed downstream of the DPF, specific heat up strategies, based on the injection pattern delay, are required in order to fasten the component warm-up. The next component developments are mainly focused on the optimization of the urea distribution inside the component, in order to further raise its efficiency, and in the reduction of the overall system backpressure. [37]

A further development is the integration of the SCR in the DPF substrate [38], [39]: this solution presents as the main strong point a faster warm-up time, due to the more adjacency to the engine exhaust, but, on the other hand, the reduced space for the urea injection and mixing and the smaller substrate length reduces considerably the system efficiency. A further drawback that has to be taken in to account is related to a mechanical weakening of the SDPF substrate, compared to a standard DPF; in fact the integration of a DPF and of a SCR on the same component requires a higher filter porosity and a thinner wall thickness.

The LNT technology, due to the different conversion mechanism, presents a nominal conversion efficiency of about 70%, thus lower compared to the SCR catalyst. On the other hand, this system is integrated in the DOC presenting lower system cost and packaging problems. The main problems related to the LNT technology is the Sulphur

poisoning also with ultra-low Sulphur fuels; this requires specific DeSO_x phases, that expose the component to high temperatures and to a rich gas mixture, in order to restore the component efficiency. However these strategies, in addition to the fuel consumption and oil dilution drawbacks, reduce also the component durability.

Starting from the next generation of EU6 engines, the adoption of at least one of the two above described technologies is mandatory in order to fulfil the NO_x emission requirements. The choice between one system and the other has to be done carefully and can be driven from different parameters, like costs, packaging issues and conversion efficiency requirements. For instance, A or B segment vehicles equipped with small diesel engines will most likely be able to fulfil emission limits by means of an LNT after-treatment system for both Euro5b and Euro6 legislations, while medium-high classes vehicles with bigger engines will need SCR systems.

Considering more stringent emission regulation, like the actual SULEV legislation in California or future emission regulations, the integration of different NO_x after-treatment devices will be mandatory in order to achieve the imposed tail pipe emission targets. Different solutions have been proposed, as an example, as reported in [6], both an LNT and an SCR were adopted, in this way it is possible to trap the NO_x in the first phases of the cycle and release them as the SCR has reached its light off temperature. In addition, ammonia formation during periodic LNT rich regeneration phases was found to be very important for the performances enhancement of the downstream SCR catalyst [40]; the produced ammonia can be adsorbed by SCR catalyst during rich phases and being subsequently available for NO_x removal under lean operation, thus creating synergies between the two after-treatment devices.

Another proposed solution [41] is the adoption of an electrical heated catalyst, plus a SPDF and a downstream SCR system. In this case, since the application was proposed for the USA market, the electrified catalyst was preferred to the LNT because, in this case, the fuel consumption increase, due to the DOC heating, was lower than the fuel consumption penalty related to a very high DeSO_x frequency, which is necessary in order to maintain the system efficiency. This aspect points out again the importance to evaluate, for every engine/vehicle/market combination, the after-treatment architecture that minimizes the overall drawbacks and achieves the best system integration.

CHAPTER II. EXPERIMENTAL APPARATUS AND TEST PROCEDURES

II.1. Introduction

The experimental activity carried out within this thesis, as previously described in the Introduction Chapter, is focused on the evaluation of three DPF different substrate materials, and of the Sulphur Poisoning Effect for a DOC. For both activities the same engine model was used, however the first activity was carried on a vehicle, in order to reproduce as much as possible the real world operating conditions, while the second was performed on a dynamic engine test bench, thus allowing a more accurate emission measurement and experimental repeatability.

This chapter presents the experimental apparatus (i.e. type of engine, type of measuring devices, etc.) which has been setup. For each of the abovementioned activities a description of the operating principle of sampling and measuring devices will be given, as well as a discussion on the main operating parameters. Finally, each test procedure adopted will be presented.

II.2. DPF Substrate investigation

II.2.1. Engine and Vehicle Characteristics

All the activity was performed on a 2.0 Liter Euro 5 Diesel Engine installed on European passenger car. The engine and vehicle technical data are reported respectively in Table II.1 and Table II.2.

Engine Characteristics	
Engine Type	Diesel 4 Stroke
Displacement	1956
Cylinder Arrangement	4 in line
BorexStroke	83,0 mm x 82 mm
Compression Ratio	16,5 : 1
Turbine	Single Stage with VGT
Fuel Injection System	Common Rail 2° gen. (CRI2.2 - 1600 bar)
Max Power	115 kW @ 4000 rpm
Max Torque	350 Nm @ 1750 rpm
Engine Inertia [kgm ²]	0.25

Table II.1 Engine Characteristics

Vehicle and Driveline Parameters	
Trasmission Type	FWD
Mass [kg]	1628
Dimensinos (lxwxh) [mm]	4830x1856x1498

Table II.2 Vehicle Technical Data

II.2.2. Tested Substrate Materials

In order to understand better the differences between the investigated materials and their influence on the DPF performances, the most important properties for DPF substrate materials will be briefly summarized hereafter:

- ***Specific Filtration Area:***

This parameter represents the total channel surface for DPF volume unit. It is computed by dividing the total channel surface area (Total Filtration Area, TFA) by the DPF volume.

$$SFA \left[\frac{1}{cm} \right] = \frac{TFA [cm^2]}{V_{DPF} [cm^3]}$$

Equation 1 Specific Filtration Area definition

A higher filtration area, theoretically, leads to higher soot loading capability. However, in most of the applications, the maximum soot loading is limited by the maximum temperatures reached inside the filters during an uncontrolled regeneration event.

- ***Coefficient of Thermal Expansion (CTE):***

The thermal expansion coefficient represents how much a material expands (or contracts) when is heated. When a thermal gradient is generated inside the DPF, the hotter region expands compressing the colder one. This generates a mechanical stress inside the component, which can eventually lead to micro cracks occurrence [42]. Therefore a smaller thermal expansion coefficient will lead to a lower thermal stress for the same thermal gradient. If the thermal stress overcomes the maximum material tensile strength the component will crack.

- ***Heat Capacity***

The heat capacity is a material property that measures the energy, that has to be provided to the object, in order to obtain a defined temperature increase. In the case of a DPF this parameter is a function of the material specific heat capacity and of DPF construction parameters which are wall porosity and cell structure. A substrate with a high heat capacity requires more energy to reach the soot combustion temperature, but on the other hand, if uncontrolled regeneration occurs, it may protect the component from damages.

- ***Thermal Conductivity***

The thermal conductivity is the property of a material to conduct heat. On one side, a high thermal conductivity allows a better distribution of the heat inside the component, leading to a better thermal shock resistance in case of uncontrolled regenerations; on the other side, it requires more energy to heat the component and perform the DPF regeneration.

- ***Maximum operating temperature:***

This parameter represents the maximum temperature at which the most important material properties are still preserved. In any case it can not be greater than the material melting temperature. For example, despite Silicon Carbide outstands a very high melting temperature (about 2200 °C), it can not be operated above 1300 °C. As a matter of fact, above this temperature, a glassy surface layer may form on DPF substrate [43], sealing the material pores and thus leading to a permanent increase of the filter back pressure.

- ***Pore Characteristic***

The pore characteristics such as volume percentage, size and distribution determine the capability to filter the soot. The porosity influences both mechanical and thermal substrate properties [44], [45], [36]: a lower number and a smaller pore dimension lead to a higher filtration efficiency and thermal robustness, but at the same time, increases the filter backpressure. As a consequence, a tradeoff between mechanical robustness and backpressure has to be found.

- ***Cell structure***

Cell structure is usually referred to the combination of cell shape (square, hexagonal, octagonal) and disposal (symmetric or asymmetric). Experimental investigations [35], [46] indicated how this parameter strongly influences the filter mechanical robustness, pressure drop and ash storage capability.

The combination of the above mentioned filter characteristics results in three main DPF properties:

- ***Filtration efficiency***

The filtration efficiency represents the property of the DPF to collect particulate and to prevent its release in the atmosphere. During the DPF loading different filtration mechanisms come in succession [30], [47]: with the empty DPF there is a deposition of soot along the pores, then there is a gradual deposition across the pores resulting in a pore sealing and at the end there is a soot deposition along the channels.

- ***Back pressure***

The pressure drop across the DPF is composed of two terms: the first one related to the clean DPF itself, the second one to the soot loading. The former results from the cell geometry, wall thickness, porosity, etc., while the latter is generated by the soot trapped into the filter. Lower back pressure leads to lower engine fuel consumption, since it reduces the gas exchange work. [48]

- ***Soot mass limit***

This parameter represents the maximum amount of soot that can be stored inside the filter without damaging the component during regeneration. Usually, the limiting factor is

represented by the maximum temperatures and gradients achieved during an uncontrolled regeneration: if these parameters exceed the material structural limits, the filter will crack.

Three different substrate materials, which were chosen among the most widely diffused for automotive applications, were compared: Silicon carbide (SiC) [49], [44], Cordierite ($2\text{MgO} - 2\text{Al}_2\text{O}_3 - 5\text{SiO}_2$) [43], [50] and Aluminum Titanate (Al_2TiO_5) [51], [52], [53], [54], [55]. The main properties of these materials are summarized in Table II.3.

Considering the DPF characteristics which are not strictly related to material properties, but to geometrical parameters (i.e. porosity, cell density and shape), some differences may be noticed between the selected samples. While Cd and AT have very similar geometrical parameters, some differences are evident in the case of SiC. It is well known from literature [45], [36], [56], [57], [58], [59] that these parameters influence both the structural and physical properties of the filter, but unfortunately it was not possible to find a SiC sample with exactly the same characteristics of the other two samples. On the other hand, it should be considered that the different geometrical parameters are usually selected by the supplier depending on the different material properties in order to obtain a filter performance capable to fulfill the requirements of a specific application. For these reasons, and for its relevance as a basis for comparison, it was decided to include also the Silicon Carbide sample in this work, although it is not perfectly identical to the other samples as far as porosity and cell density are concerned.

The most significant differences between the selected materials, and in particular between SiC and the other two, lay in the thermal expansion coefficient and in the thermal conductivity. These two material characteristics are one order of magnitude higher for Silicon Carbide, compared to Cordierite and Aluminum Titanate substrates.

The high thermal expansion coefficient represents undoubtedly the Achilles' heel of Silicon Carbide due to the high mechanical stress generated during the regeneration process. In order to overcome this limit, SiC components are usually made up of small, square segments instead of a monolithic structure. This leads, however, to a lower specific filtration area and to a higher backpressure.

	[]	SiC	Cd	AT
Porosity	[%]	42 +/-3	48	49 +/-1
Filter density	Kg/l	0.84	0.7*	0.66
Young's module	GPa	58.1	9.3	1.51
CTE (Coefficient of Thermal Exp)	1/°C x 10 ⁻⁷	45	5.4	10
Thermal conductivity	@500 °C (W/mK)	10-20	0.8	0.48
Volumetric Heat Capacity	@500 °C (J/cm ³ °C)	3.63	2.79	3.6
Melting Temperature	°C	2200	1450	>1600
Modulus of Rupture	MPa	13.7	4.67*	1.5
Cell density for this application	cpai/mil	350/11	300/16	300/13
Cell shape for this application	-	OS	HAC	ACT

Table II.3 Materials properties (values* were not directly provided by the supplier but taken from literature [31]).

II.2.3. Experimental Set-Up and Test Procedure

II.2.3.1. Experimental investigation of exhaust backpressure and fuel consumption

Firstly, the three different substrates were characterized over the NEDC to evaluate the impact of the different substrate material properties on engine backpressure and thus on fuel consumption. A NEDC cycle was then performed for each component at three different soot loadings: 0, 8 and 11 g/l measuring CO₂ emissions. During the loading phase the filters were soot loaded under real world operating conditions on the road, while inhibiting the regeneration: the DPF was periodically dismantled and weighted in order to check the soot loading level reached.

Figure II-1 illustrates a scheme of the chassis dyno adopted for the tests. As shown in the picture, the drive wheels are connected to an electric driven Zoolner 48" roller that allows to reproduce, for each driving profile, the vehicle rolling resistance according to the vehicle coast down coefficients. The tail pipe exhaust gases are diluted with ambient air in a CVS (Constant Volume Sampling) system. The diluted exhaust gases and the ambient air are then sampled and stored in specific bags, at the end of the cycle the pollutants in each bag is measured through a Horiba MEXA 7400 analyzer. All the sample line is heated in order to avoid condensation of acid gases (NO_x, SO_x), moreover specific filters are set in order to remove the particulate matter, that would damage the gas analyzer. The particulate emission measurement is then performed in a second line, where the exhaust flow is

further diluted in order to prevent particle collision and nucleation. The flow is then forced to pass through specific filters, that once weighted, allow the calculation of the total emitted particulate mass (PM). On the same line, a Horiba MEXA-1000 condensation particulate counter was installed in order to measure the total number of emitted particle (PN).

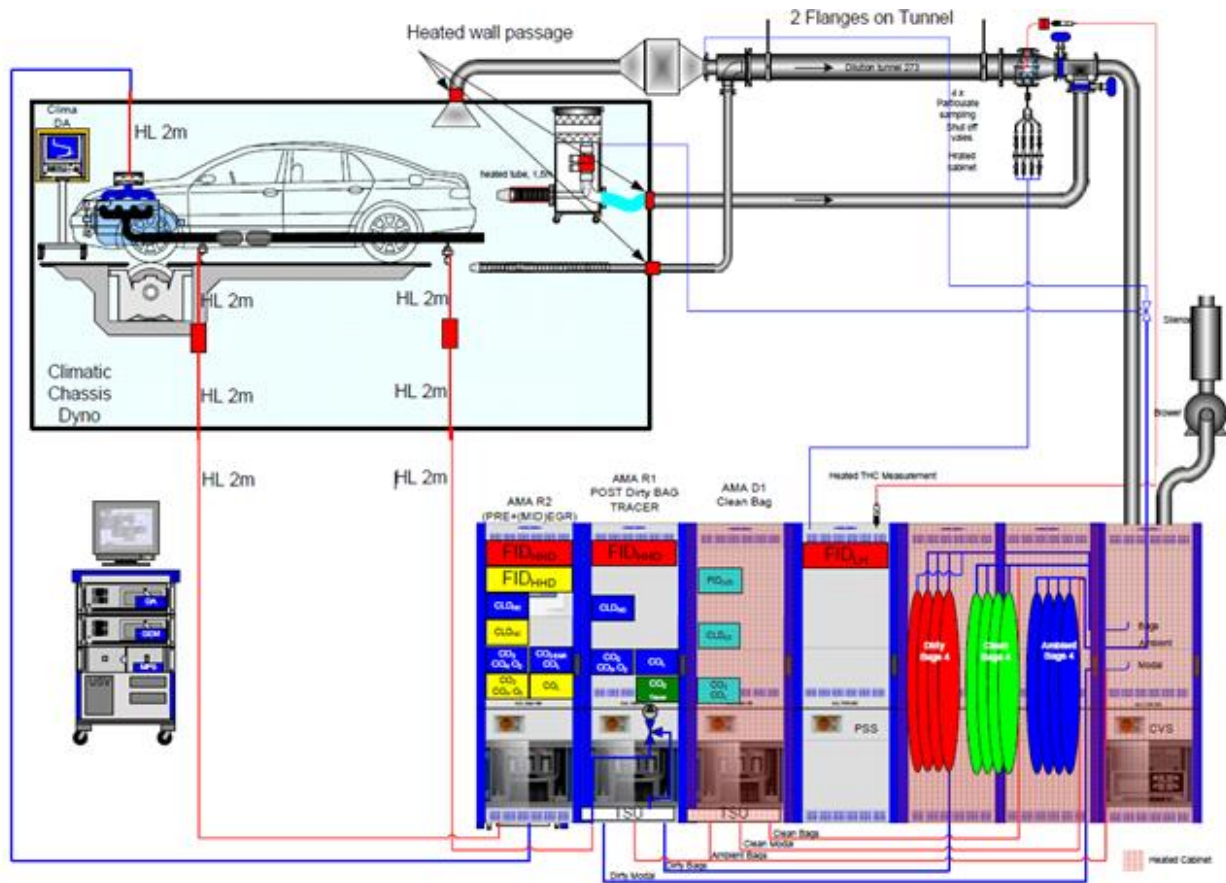


Figure II-1 Roller Bench Scheme

Figure II-2 shows a comparison of the backpressures over the driving cycle stationary phases at 50/70/100 km/h, while Table II.4 reports the fuel consumption differences between the performed cycles. The Silicon Carbide demonstrated, due to its segmented structure, the highest back pressure between the investigated substrates. The Titanate Aluminum and Cordierite backpressures were comparable for the empty components, while lower backpressure was observed by Titanate Aluminum when the components were loaded at 11 g/l. Although the backpressure differences were not negligible, both with empty and with loaded components, the impact on fuel consumption was not appreciable (Table II.4).

During the tests the exhaust gas temperatures at the DOC inlet and at the DPF outlet were also monitored. Figure II-3 illustrates, by way of example, the results obtained for empty DPFs. Even though temperature levels at the DOC inlet are quite close to each other for all the substrates, the temperature trends at the DPF outlet show remarkable differences: in particular the Silicon Carbide's higher thermal conductivity leads to significantly lower gas temperatures at the DPF outlet, with temperature levels up to 30°C lower than those reached by Cordierite and Aluminum Titanate. As discussed before, this may significantly influence the conversion efficiency of an SCR system installed downstream of the DPF, thus requiring a stronger heating strategy, that would result in a higher fuel consumption penalizations.

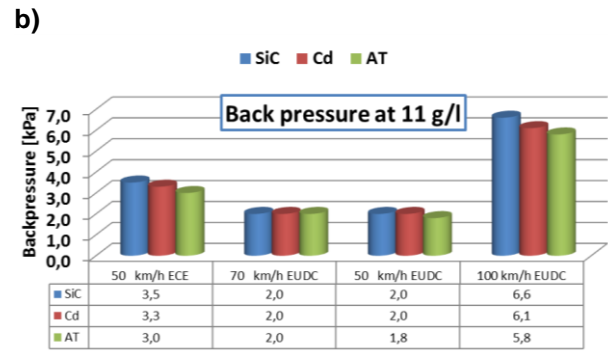
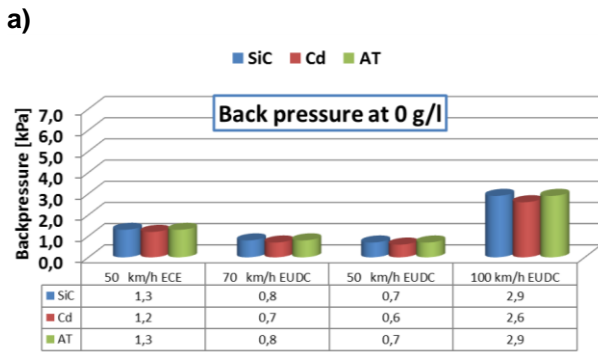


Figure II-2 a) Measured backpressure over the NEDC cycle at 0 g/l
b) Measured backpressure over the NEDC cycle at 11 g/l

DELTA FUEL CONSUMPTION			
	0 g/l	8 g/l	11 g/l
SiC	0,0%	-1,8%	0,0%
Cd	0,0%	0,0%	0,0%
AT	-1,8%	NA	1,8%

Table II.4 Delta fuel consumption, compared to SiC 0 g/l, over the NEDC cycle

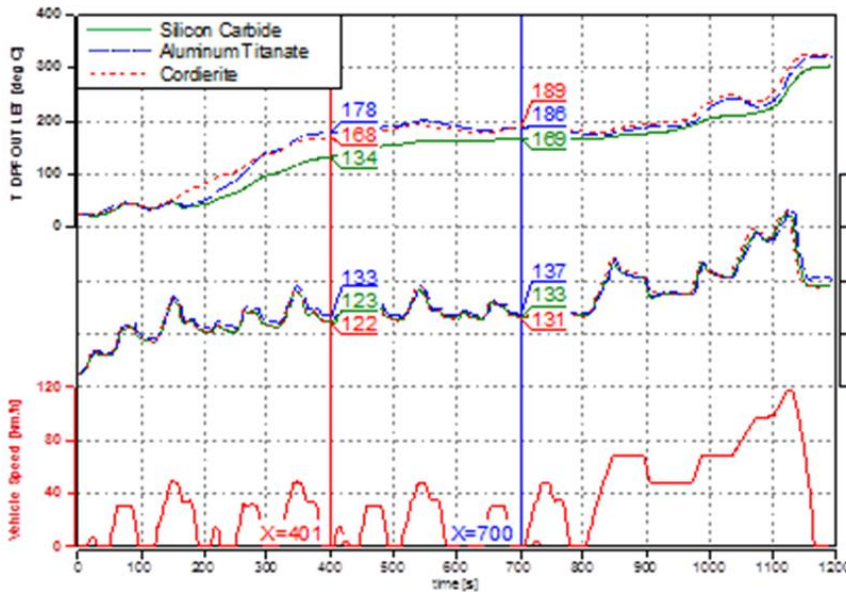


Figure II-3 Exhaust temperatures at the DOC inlet and at the DPF outlet over NEDCs carried out with soot empty DPFs.

Filter regeneration

After the above mentioned tests, regeneration tests aiming to define the soot mass limit for each substrate were performed. For this activity the filters were instrumented with 20 thermocouples as shown in Figure II-4.

The filter loadings were performed over an extraurban driving profile, imposing a maximum vehicle speed of 70 km/h and an average speed of 50 km/h: during this loading phase the regeneration was inhibited and the DPF was weighted periodically.

Two different regeneration procedures were tested: in the first one the regeneration was performed over the NEDC, while in the second one a so called “Drop To Idle” (DTI) maneuver was performed. In the first step, a controlled regeneration in an urban driving condition is simulated, since the regeneration ends at the first cut off of the extra-urban portion of the driving cycle, as shown in Figure 3a. The Drop To Idle (DTI) maneuver is performed with the vehicle stopped as described hereafter (see also Figure II-6b): the engine is operated at 2000 rpm x 0 bar BMEP until the central thermocouple of the rear DPF section (thermocouple # 10 in Figure II-4) reaches 620 °C: in that moment the accelerator pedal is released and the remaining part of the regeneration is performed at idle. This indicates an uncontrolled regeneration, since, after the soot combustion begins, the exhaust mass flow is dramatically reduced, and as a consequence, the heat which is generated by soot oxidation cannot be dissipated through the exhaust mass flow, but is almost completely absorbed by the substrate. Figure II-6 shows the temperatures trends during the abovementioned two regeneration conditions for a Silicon Carbide substrate at the same soot loading of 10 g/l. The substrate temperatures in the front and middle sections are very close to the exhaust temperature measured by the ECU (solid line), while the temperature peak occurs in the rear section (thermocouple # 10).

The different material properties play a fundamental role in determining the temperature profiles inside the substrate. The temperatures measured over the horizontal diameter of the rear DPF section during a DTI regeneration event, with same soot loading of 8 g/l, are shown in Figure II-5. The data are referred to the time when the temperature peak is reached (see Figure II-6b). This picture clearly points out the effect of different thermal conductivity on the temperature distribution inside the substrate: while the Silicon Carbide has a relatively uniform temperature profile, Cordierite and Aluminum Titanate show a sudden temperature drop towards the external thermocouple ring and, consequently, higher temperatures in the inner section of the component.

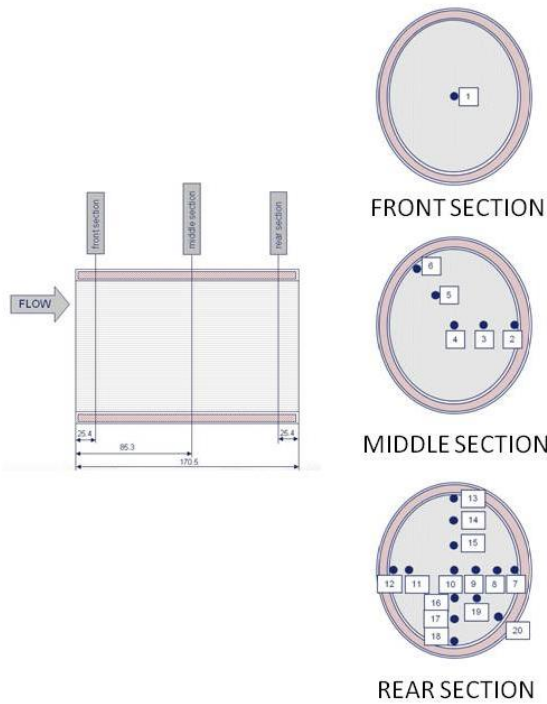


Figure II-4 Thermocouples locations inside the DPF

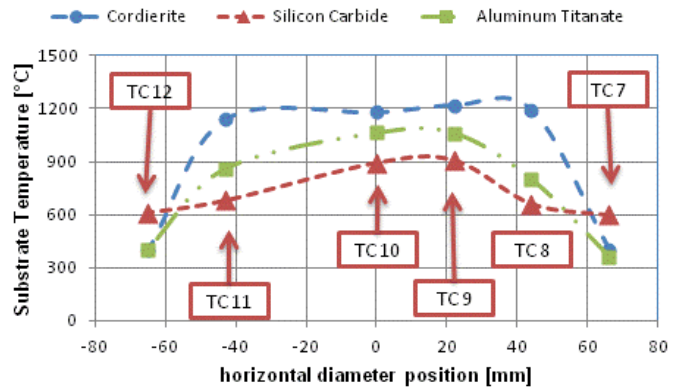


Figure II-5 Temperature trends over the horizontal diameter of the rear DPF section (Thermocouples # 7 : 12 in Figure II-4) during a DTI event.

a)

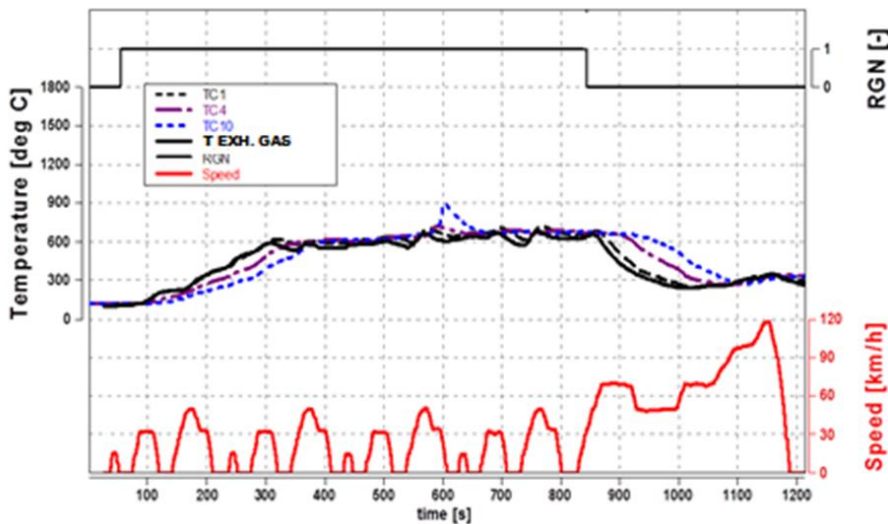
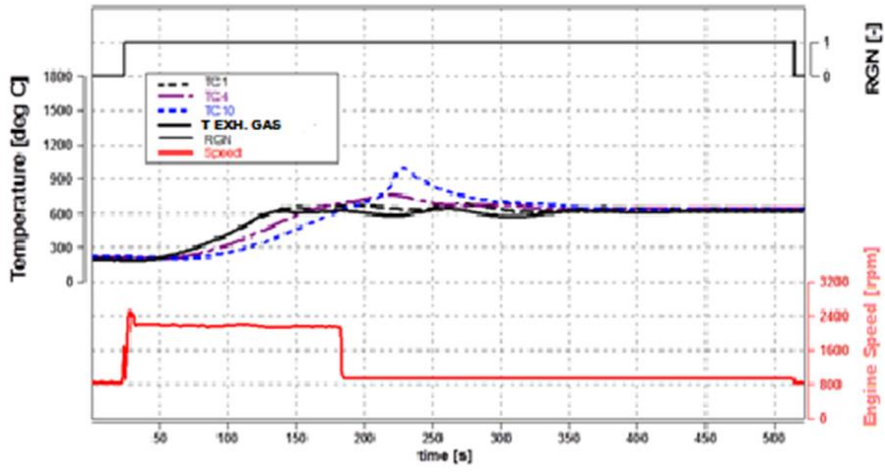


Figure II-6 Temperature trends during regeneration events on a Silicon Carbide DPF at a soot loading of 10 g/l over NEDC (a) and drop to idle (b). The signals TC1, TC4, TC10 refer to the thermocouples # 1, 4, 10 shown in Figure II-4. The solid line labeled as Exh_tPFI

b)



II.3. DOC Sulphur Poisoning Investigation

II.3.1. Experimental Set-up

As discussed in the introduction of the chapter, for this activity the same engine model of the DPF substrate investigation was used, but the activity was carried on an AVL high-dynamic test bed. The facility is equipped with an ELIN AVL APA 100 cradle-mounted dynamometer allowing NEDC simulation, featuring maximum torque and power of respectively 525 Nm and 200 kW, as well as a maximum speed of 12000 rpm. This test bench is capable of realizing full four-quadrant operation with high speed and torque dynamics, including simulation of zero torque and gear-shifting oscillations in the drivetrain.

The instantaneous fuel consumption was measured through an AVL KMA 4000 system; exhaust gas were sampled at two different locations in the exhaust, at the engine outlet by means of an AVL AMA i60 gas analyzer and at the DPF outlet by means of a V&F Mass Spectrometer, as reported in Figure 1. It should be noted that AVL System-One engine test bed for S poisoning tests was adopted.

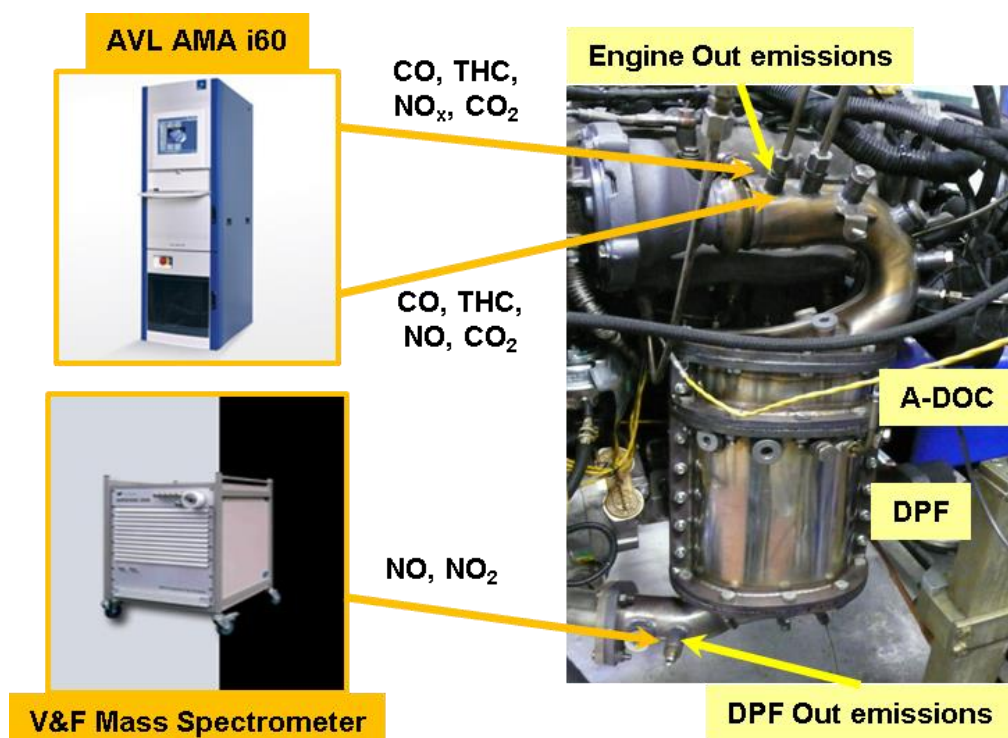


Figure II-7 Exhaust emission measurement layout [60]

The AMA i60 features two simultaneous sampling lines, thus allowing the measurement of pollutant species in two locations along the exhaust line such as, for instance, at engine outlet and DPF outlet. Simultaneous measurement of the NO_x split in terms of NO and NO₂ species. Moreover, gas temperatures and pressures in the most important locations of the exhaust and intake systems of the engine (i.e. upstream and downstream of the compressor and turbine, of air and EGR cooler, etc.) were measured by means of K-type thermocouples and piezoresistive pressure transducers respectively.

All of the described measurement devices are controlled by a PUMA Open 1.3.2 automation system, which also includes ISAC 400 software for the simulation of vehicle (road load, road gradient and moments of inertia of the driveline components that are not physically present on the test bed) and driver behavior (use of clutch, accelerator pedal and gear shifting), thus allowing the user to reproduce the driving cycles which are usually carried out on the whole vehicle on the chassis dynamometer. The simulated vehicle was a European Sedan passenger car with manual transmission featuring an equivalent inertia of about 1600 kg.

Tested component was a cc(DOC-DPF) catalyst. Components were installed inside a dismountable canning, as shown in Figure II-7, allowing an easy switch between different components.

The main characteristics of tested after-treatment components installed in the dismountable canning are listed in Table II.5. The execution of the NEDC was repeated at least three times, in order to check the repeatability of the results [60].

Aftertreatment components		
Technology	DOC	DPF
Substrate Volume [dm³]	1.36	3.16
Cell Density [cpsi]	400	300
PGM [g/ft³]	120	5
(Pt/Pd/Rh)	(2:1:0)	(1:0:0)

Table II.5 After-treatment system characteristics

Special fuel with increased sulfur content was selected for this activity namely S500, although the lab measurements evaluated the sulfur content of 622 ppm. It is worth mentioning that the temperature measured in this study is the gas temperature, not the monolith, although in previous activities it was proven that through simulations the monolith temperature can be estimated

II.3.2. Test Procedure

II.3.2.1. *Sulfur Poisoning Test Procedure*

A diesel fuel containing 622 ppm of sulfur was chosen for poisoning the aftertreatment system. A specific procedure was adopted in order to poison the exhaust system: this procedure consisted of one elemental cycle, described in Table II.6, with a duration of 1h; 4 different poisoning levels were achieved by repeating the elemental cycle 1,4,7 and 10 times which resulted in 1.62, 6.48, 11.34 and 16.2 gr of engine out sulfur, respectively, Table II.7

Elementary cycle				Total
Engine speed [rpm]	1500	1750	2000	-
Engine load - BMEP [bar]	2	5	5	-
S-content [ppm]	622	622	622	-
Duration [min]	30	20	10	1 hour S poisoning
Fuel consumption [kg/h]	1.65	3.34	4.00	-
S Engine out [g]	0.513	0.692	0.415	1.620

Table II.6 Elementary cycle for poisoning the aftertreatment system

Sulfur content	Level 1	Level 2	Level 3	Level 4
g	1.62	6.48	11.34	16.2
g/l	0.36	1.43	2.51	3.58

Table II.7 Levels of sulfur poisoning

During the elemental cycle, a maximum exhaust gases temperature of 360°C, measured at DOC inlet, was registered. The theoretical quantity of sulfur which was burnt, is

calculated on the basis of the fuel consumption (measured by means of a AVL fuel Balance 733S) and the fuel sulfur content.

II.3.2.2. *cc(DOC+DPF) performance characterization test procedure:*

The evaluation of the efficiency of the exhaust system was carried out on cold NEDC; the NEDC was repeated at least 4 times for repeatability check. During each driving cycle pollutant emissions were sampled downstream of the turbine (Engine Out position), at DOC outlet or DPF outlet. The tests were carried out first on fresh components and then at each poisoning step.

II.3.2.3. *De-sulfation Test Procedure:*

A specific procedure was adopted in order to regenerate cc(DOC+DPF). During the tests the effective sulfur quantity which was released by DOC was measured by means of a mass spectrometer connected at its outlet.

II.3.2.4. *cc(DOC+DPF) light off and light out test procedure:*

A specific procedure was adopted in order to investigate the effects of both sulfur poisoning and exhaust system regeneration on DOC light-off and out curves. Tests were carried out at 3 operating points in order to investigate the effects that different exhaust gases space velocities may have on light-off curves. The operating points are listed in Table II.8.

Characteristics of operating points			
Engine Speed [rpm]	1500	2000	2500
Engine Load - BMEP [bar]	3	3	2
Space Velocity [1/h]	50000	100000	130000

Table II.8 Operating points

The procedure consisted of 4 steps which are depicted in Figure II-8. In the first step, increase of engine load from 0.1 [bar] of BMEP up to target BMEP is performed in 600 seconds; at step 2, engine is run at target operating point for 150 seconds; Next, the engine load from target BMEP is decreased down to 0.1 [bar] of BMEP in 600 seconds

and finally, engine is run at 0.1 [bar] of BMEP till DOC CO and HC abatement efficiencies reach a minimum level of 30%.

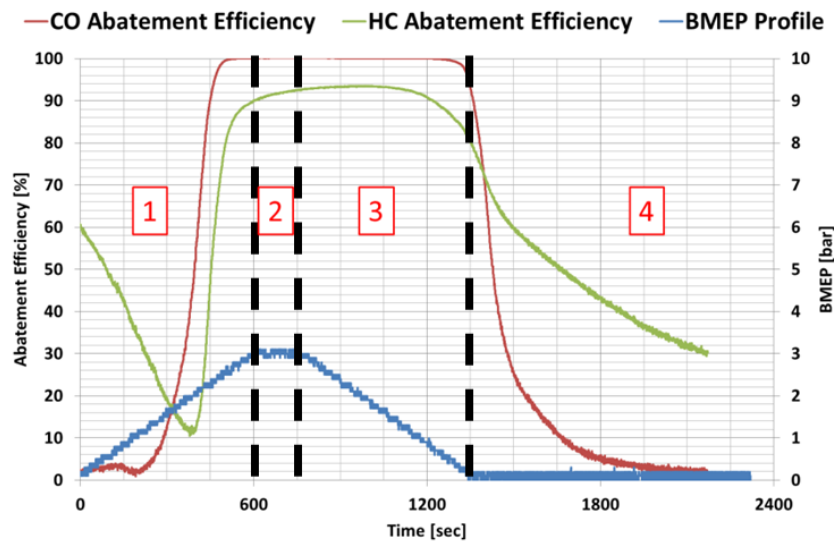


Figure II-8 Light-off procedure, transient ramp cycle

This engine ramp cycle was designed to cause a gradual increase in exhaust gas temperature in order to obtain an accurate catalyst light-off curve and allow the determination of any impact of exhaust gas chemical composition on catalyst performance [12].

An example of light-off curve obtained through transient ramp cycle is depicted in Figure II-9. Light-off temperature is referred to the temperature at which more than 50% of the engine out emissions is being converted through ramp up, heating, phase [61]. It is worth mentioning that the hysteresis effect observed in Figure II-9 can be attributed to a thermal effect [62] and CO self-inhibition, [61], [63] and [64], while the latter plays the main role. During the heating phase, at low inlet gas temperatures the CO oxidation is self-inhibited due to high CO surface coverage and less vacant sites for oxygen and other species. When the temperature is raised, CO desorbs and more active sites become available. On the other hand, during the cooling phase, firstly at high temperatures the initial surface coverage of CO is low and it increases as the inlet gas temperature is reduced, hence CO inhibition occurs again. Once the catalyst has been lit-off, the heat released from the chemical reactions promotes the reaction and high CO desorption rates counteract the CO self-inhibition effects [62].

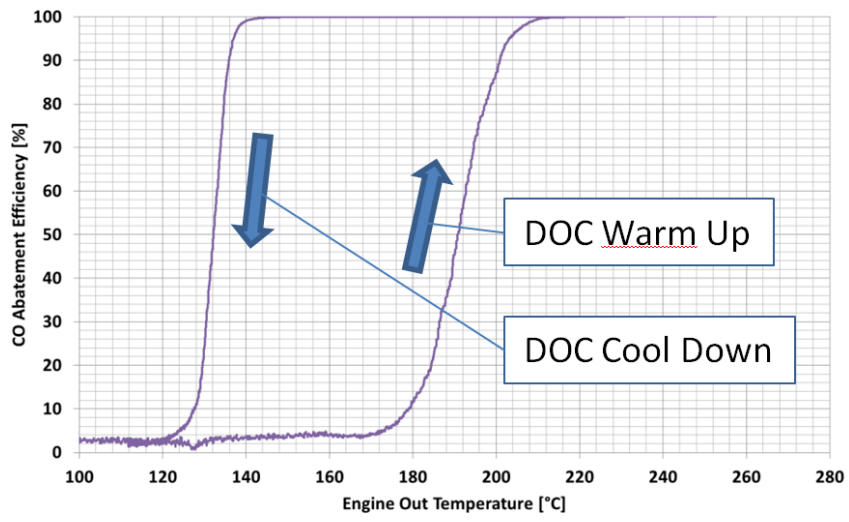


Figure II-9- CO light-off curve obtained with the aid of transient ramp cycle

CHAPTER III. ENGINE AND DPF MODEL SET UP

III.1. INTRODUCTION

Starting from the experimental activity an engine and DPF model was set up in order to extend the experimental results to different conditions and to be able to foresee the system reactions by changing some parameters or environmental conditions. As an example it was possible to extend the experimental results achieved over the NEDC also to other driving cycles. In this chapter a short description of the model set-up will be provided.

III.2. 1D ENGINE MODEL SET-UP

In order to assess the impact of back pressure, due to different soot loadings, on vehicle fuel consumption over various driving cycles, numerical simulations were performed by means of a one dimensional fluid-dynamic engine model “GT-Power”. The general features of the simulation code are described in details in [65], [66], while the construction of the model and the validation process are described more in details in [67] and will be only briefly summarized hereafter. The baseline model construction requires a careful and detailed schematization of the engine and of the intake and exhaust system geometries, as well as accurate and extensive experimental data, which have to be carefully analyzed in order to properly set the heat transfer and friction loss coefficients, and combustion heat release profiles as well as to estimate the engine friction. In particular, as far as the combustion model is concerned, the heat release profiles obtained from the analysis of experimental in-cylinder pressure traces were used for the baseline model, while the engine friction losses were evaluated through motoring tests. The heat exchange process inside the intake charge coolers (intercooler and EGR coolers) was modeled by means of experimentally derived performance maps, which provide cooler effectiveness as a function of the gas flow rate. The pressure drop across the coolers was calibrated using experimental data that were acquired during experimental steady state tests. The whole after treatment system downstream of the turbine was simulated by means of an orifice which was calibrated in order to reproduce the different back pressures experimentally measured for each after treatment component and each soot load condition. The simulation results were then compared with the experimental results under both steady state and transient operating conditions, as reported more in details in [67]. Afterwards,

since simulation speed is of primary importance when running long transients such as a driving cycle, with the need of comparing several different configurations for the engine or the vehicle, a simplified or Fast Running Model (FRM) was derived from the detailed model, as described in [32]. Basically, a Fully Physical FRM is similar to the original detailed engine model, but with a coarser discretization of the flow path: the detailed engine model reduction process basically consists of lumping volumes together, thereby reducing the number of flow volumes and, consequently, increasing the time step size. Obviously, the total volume and the total heat transfer surface were preserved in each component. The less detailed flow path causes a certain loss in fidelity of wave dynamics. However, this drawback affects high frequency phenomena such as acoustics, while the main fluid-dynamics phenomena are still well predicted. Thanks to the larger volumes, the discretization length (dx), which is the length of the 1D volumes, could be raised significantly. The increased dx leads to larger time-steps (dt): in fact the numerical code explicit solver automatically chooses the larger time-step which satisfies the Courant condition at the same time on every sub-volume in the model, based on their length. Both the detailed and the FRM were then tested on a transient run, an NEDC driving cycle. The FRM proved to be more than 20 times faster than the detailed model, achieving close to real time execution, while preserving a high fidelity. Figure III-1 shows, as an example, the back pressure over the NEDC for the empty Cordierite filter, for which a very good agreement between the simulated and experimental pressure traces can be noticed.

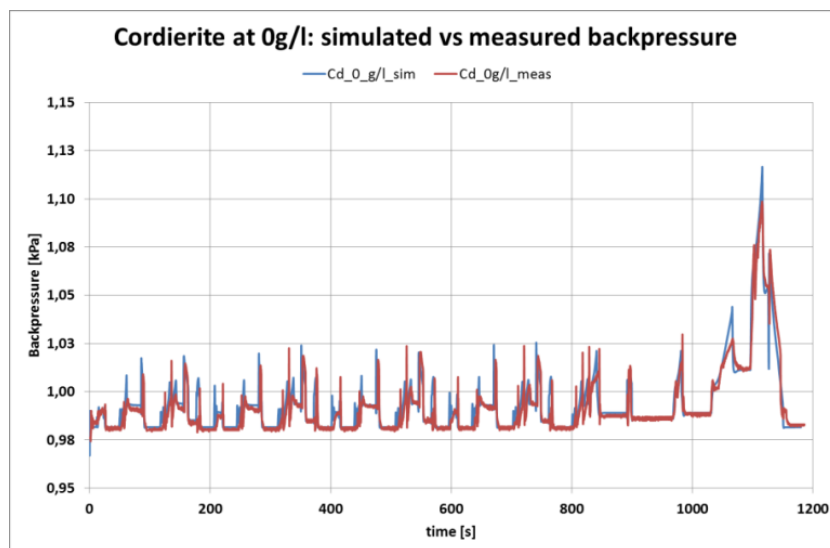


Figure III-1 Comparison between experimental and measured backpressure in the case of empty Cordierite component

A back pressure increase may have a negative impact on the fuel consumption since it increases the gas exchange work, and may shift the operating point of the turbocharger to a lower efficiency area. The 1-D engine model allows taking into account both these effects, providing an accurate prediction of the fuel consumption increase as a function of the back pressure. In order to evaluate these effects over different driving conditions, the following driving cycles were simulated:

NEDC: this cycle (see Figure III-2) was adopted to provide a model validation with the experimental data and because it represents the actual reference cycle for the type approval procedure in Europe.

ARTEMIS URBAN and ROAD: these two cycles (see Figure III-3 and Figure III-4) represent typical real world urban and extra-urban driving conditions [68] [69].

WLTC: the Worldwide Light vehicle Test Cycle is a test cycle for the determination of emissions and fuel consumption from light-duty vehicles, which is being developed under the aegis of the United Nations, and should better reflect the real conditions in which cars are being used nowadays. It should replace the NEDC procedure as a matter of urgency, if possible by 2017. The cycle is characterized by four phases: Low, Middle, High, and Extra High with maximum speeds lower than 60, 80, 100, and 130 km/h respectively (see Figure III-5).

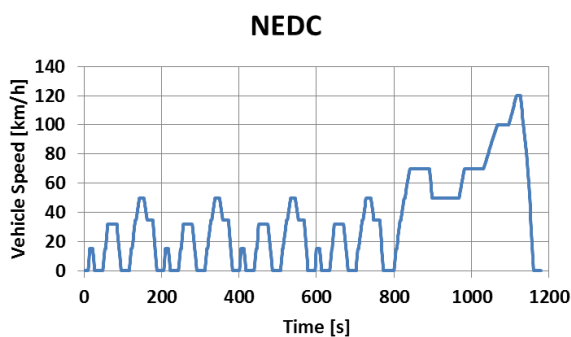


Figure III-2 NEDC driving profile

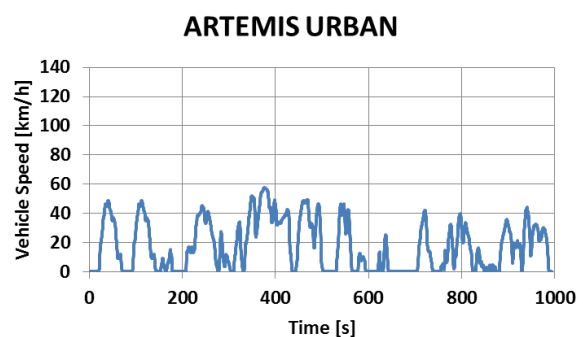


Figure III-3 Artemis Urban driving profile

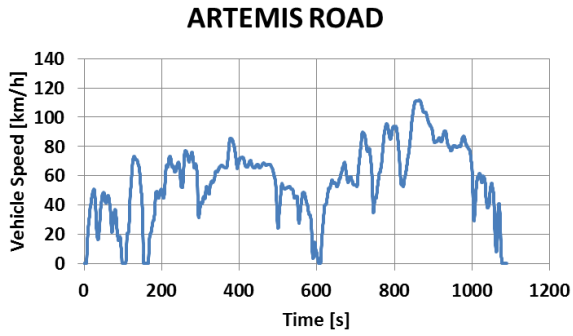


Figure III-4 Artemis Road driving profile

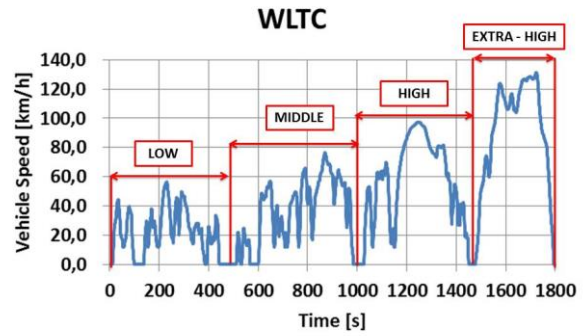


Figure III-5 WLTC driving profile

Figure III-6 shows a comparison of the vehicle accelerations and speeds over the different driving cycles. This picture points out how the NEDC cycle is characterized by lower and uniform vehicle dynamics (constant acceleration), compared to the other driving cycles, while the Artemis Urban instead presents the highest acceleration values, and the WLTC the highest vehicle speeds.

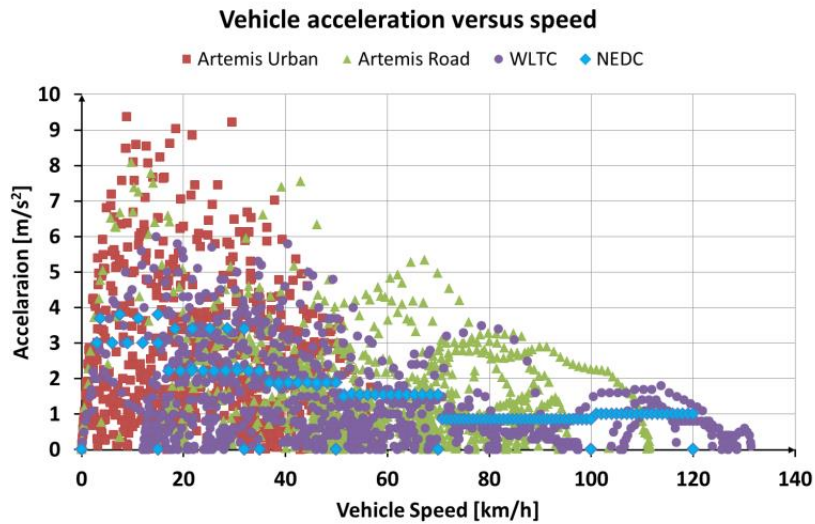


Figure III-6 Vehicle acceleration versus speed for the different driving cycles

Three different back pressure levels were simulated, including values also significantly higher compared to those measured in the real cycles. This option was chosen in order to evaluate the effects of the possibility of increasing the maximum filter soot loading and to

take into account the possible adoption of a NO_x after treatment device placed downstream the DPF, for instance an SCR.

The fuel consumption increments as a function of the exhaust back pressure, over the different driving cycles, are reported in Table III.1. While the fuel consumption increment over the NEDC cycle was generally negligible (lower than 1%, except for the highest back pressure level), as well as for the Artemis Urban and Road, over the WLTC a significant fuel consumption increment (up to 4% for the highest back pressure level) could be noticed. This result has to be attributed to the higher maximum vehicle speed (up to 130 km/h) and to a more severe gear shift schedule which is prescribed by the test procedure. These two factors lead the engine to work at higher speed points where the drawbacks of an increased back pressure are more significant. As a matter of fact, if the fuel consumption increments are evaluated separately on the different phases of the WLTC, as reported in Table III.2, the highest fuel consumption increment (up to +8% for the highest back pressure level) are registered for the “Extra-High” section, where the highest engine speeds are reached.

FUEL CONSUMPTION INCREMENTS				
Cycle	Backpressure	+3 kPa	+6 kPa	+9 kPa
ARTEMIS URBAN	0,29%	0,58%	0,85%	
ARTEMIS ROAD	0,22%	0,66%	1,09%	
WLTC	1,34%	2,68%	4,02%	

WLTC FUEL CONSUMPTION INCREMENTS				
WLTC Phase	Backpressure	+3 kPa	+6 kPa	+9 kPa
Middle	0,65%	1,37%	2,09%	
High	0,72%	1,46%	2,16%	
Extra-High	2,58%	5,58%	8,00%	

Table III.1 Percentage Fuel Consumption increments as a function of backpressure

Table III.2 Percentage Fuel Consumption increment for the different WLTC Phases

III.3. DPF MODEL SET UP

A commercially available code, Gt-Power from Gamma Technologies [65], was used in order to model the regeneration process inside the diesel particulate filter and in particular the substrate temperature during the regeneration.

Different filter models were taken in to account for the analysis: from a complete 3D to a 0D model. The adoption of a 3D model requires providing the real soot distribution inside the filter. Since the soot distribution depends on a lot of factors, it is not possible to estimate this parameter without specific experimental tests. In particular it would be necessary to perform a CFD study in order to evaluate the gas flow distribution at filter

inlet and to develop an accurate loading model that has to be verified with a filter tomography. Since a so detailed analysis was not possible, the use of a 1D model was taken in to account. In this case the soot distribution inside the filter was hypothesized according to the current literature, but also in this case, without the support of specific experimental data it was not possible to achieve a satisfactory model accuracy. Nevertheless, in addition to the necessity of specific experimental tests, the simulation time required for the different model types has also to be taken in to account; Figure III-7 shows the ratio between the simulation time and the real time for the three different models: a 3D model requires up to 215 times the real regeneration duration while a 0D model runs in half of real time. For the computation a Intel-Core i7 Processor with a 2.3 GHz clock frequency and a 4 GB RAM memory was used.

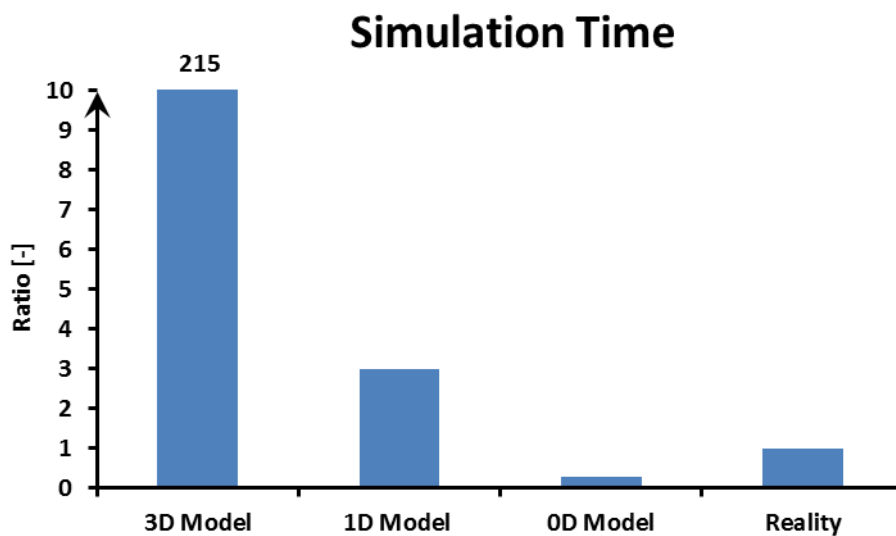


Figure III-7 Simulation time comparison between different model types.

Evaluating the above mentioned issues and considering that the main model purpose was to predict the temperature peak in the filter substrate, varying the regeneration conditions and substrate material properties, a 0D model was chosen.

.A complete description of the model characteristics is provided in [70] and [65], hereafter only a short overview of the main governing equations will be provided.

The implemented model considers both thermal and catalytic reactions, applied to a soot-cake and to a substrate layer. The first one represents the soot trapped inside the filter pores, while the second takes in to account the soot deposited along the filter walls.

The regeneration model is based on the carbon oxidation reaction reported in Equation 2 and Equation 3, for thermal and catalytic reactions respectively. In both equations the

$f_{CO_{thm}}$ coefficient allows to define the percentage of CO that is generated from the carbon oxidation.

$$C + \left(1 - \frac{f_{CO_{thm}}}{2}\right) O_2 = f_{CO_{thm}} * CO + (1 - f_{CO_{thm}}) CO_2$$

Equation 2 Thermal reaction

$$C + \left(1 - \frac{f_{CO_{cat}}}{2}\right) O_2 = f_{CO_{cat}} * CO + (1 - f_{CO_{cat}}) CO_2$$

Equation 3 Catalytic reaction

The soot oxidation rate is defined by Equation 4 and takes in to account the substrate surface area (S_p), the gas density (ρ_w), the oxygen mass concentration (Y_{O_2}), the molecular weight of carbon (M_C) and oxygen (M_{O_2}). The two coefficients K_{thm} and K_{cat} , based on the Arrhenius law, consider instead the dependency of the reaction speed with the substrate temperature for thermal and catalytic reactions respectively.

$$\dot{r}_{soot} = - (K_{thm} + K_{cat}) * S_p * \rho_w * Y_{O_2} * \frac{M_C}{M_{O_2}}$$

Equation 4 Soot oxidation rate

$$K_{thm} = A_T * T * e^{\left(\frac{E_{a_{thm}}}{R*T}\right)}$$

Equation 5 Thermal reaction coefficient for soot oxidation rate

$$K_{cat} = A_T * T * e^{\left(\frac{E_{a_{cat}}}{R*T}\right)}$$

Equation 6 Catalytic reaction coefficient for soot oxidation rate

Since the 0D model considers the filter as a unique thermal mass, it only provides an average substrate temperature. As consequence a calibration coefficient was used to take in to account the 3D non uniform soot distribution inside the filter, that leads to higher temperature peaks in specific filter sections. This coefficient was computed on the basis of the ratio between the maximum temperature measured inside the filter and the weighted average substrate temperature over different regenerations; Figure III-9 shows as an example a DTI event in an AT Filter: in the picture the red dashed line represents the

weighted average filter temperature, while the continuous lines are the temperatures in different filter sections according to the thermocouple scheme of Figure II-4, Figure III-8 shows as an example, for a 8 g/l DTI in an AT Filter, the average filter temperature predicted from the model (dashed blue line), the corrected filter temperature (blue line), obtained multiplying the average filter temperature for the calibration factor, and the maximum temperature measured inside the filter (red line).

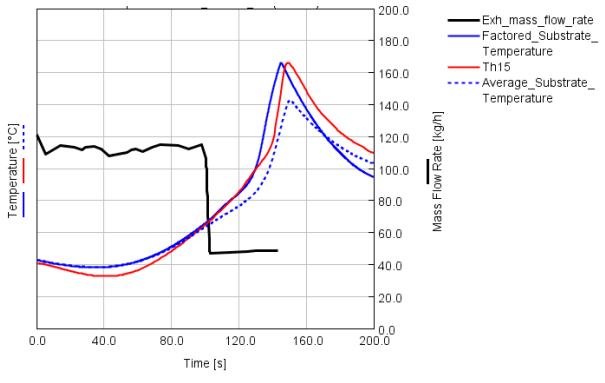


Figure III-8 Comparison between model average filter temperature, factored temperature and maximum substrate temperature measured in a DTI event

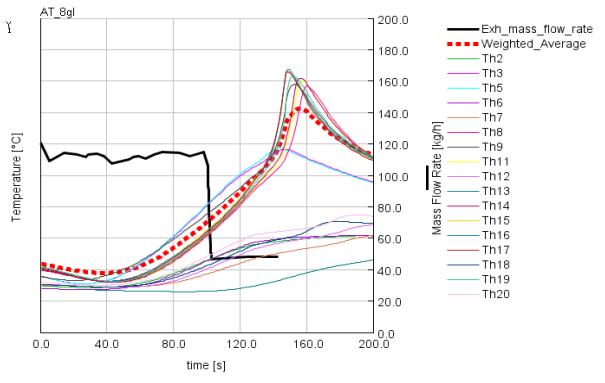


Figure III-9 Measured and weighted average DPF substrate temperature during a DTI event

Once computed the calibration factor and once performed a first model calibration, it was possible to compute the maximum filter temperature varying the soot loading and the substrate material.

Figure III-10 - 15 show the model output when applied at different drop to idle tests, considering different soot loadings and substrate materials. In the pictures the dashed red line represents the model output, while the continuous lines show the Thermocouples (see Figure II-4) where the maximum temperature were reached. In all the cases the model shows a good agreement with the experimental data; it's worth to recall that the filter loading was performed on the road, with different environmental conditions and driving profiles, thus introducing a higher variability factor compared to tests performed in a test bench with a defined soot composition. .

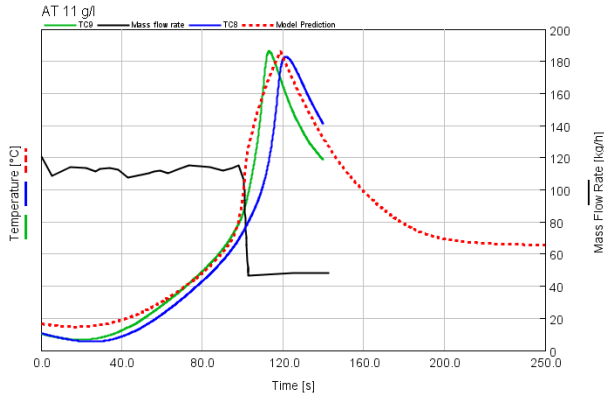


Figure III-10 Comparison between model prediction and substrate Temperature in a Aluminum Titanate 11g/l DTI

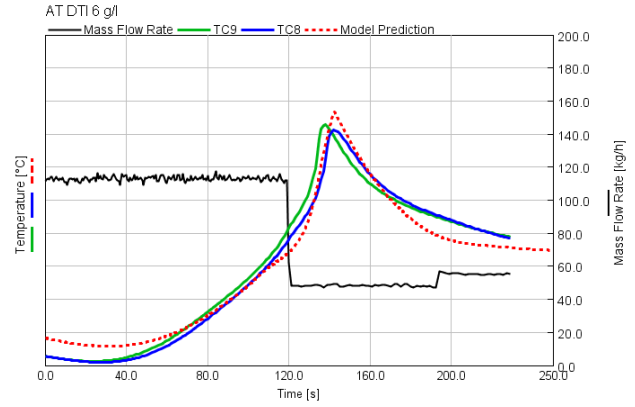


Figure III-11 Comparison between model prediction and substrate Temperature in a Aluminum Titanate 06 g/l DTI

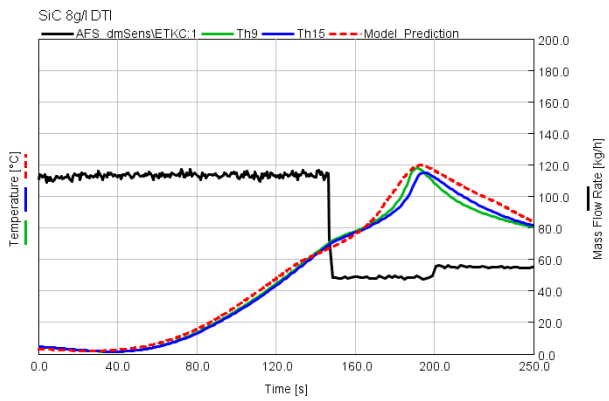


Figure III-12 Comparison between model prediction and substrate Temperature in a Silicon Carbide 08 g/l DTI

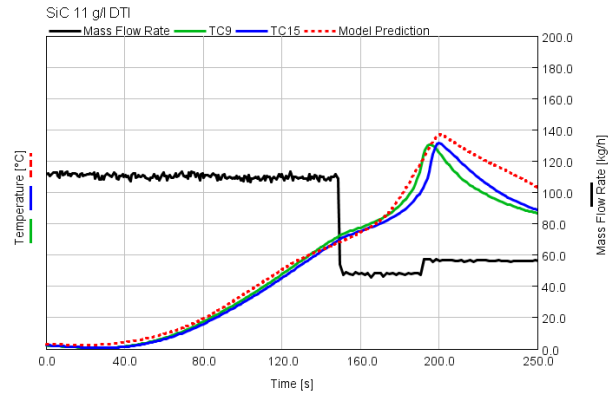


Figure III-13 Comparison between model prediction and substrate Temperature in a Silicon Carbide 11 g/l DTI

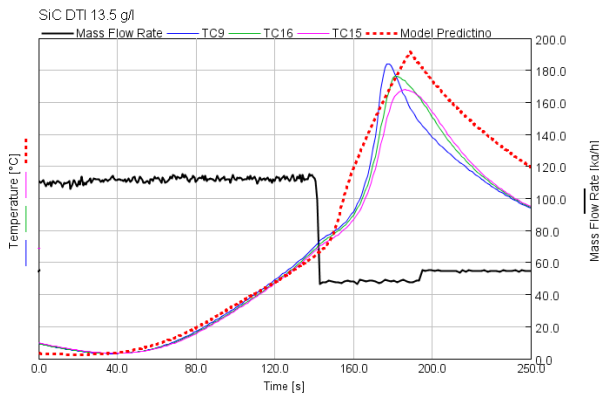


Figure III-14 Comparison between model prediction and substrate Temperature in a Silicon Carbide 13.5 g/l DTI

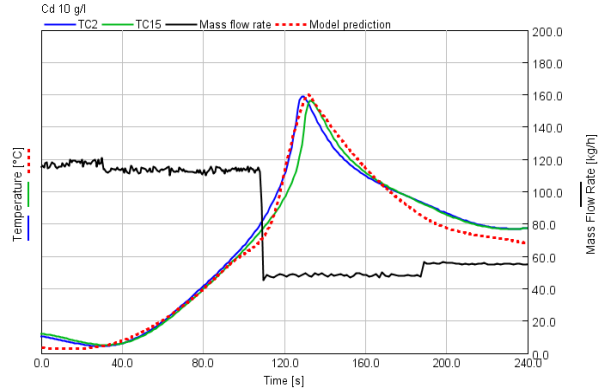


Figure III-15 Comparison between model prediction and substrate Temperature in a Cordierite 10 g/l DTI

CHAPTER IV. SOOT MASS LIMIT IMPACT ON FUEL CONSUMPTION AND OIL DILUTION

IV.1. INTRODUCTION

In this chapter the main outputs of the soot mass limit tests will be firstly discussed, then, considering the 1D Engine and DPF model results, it will be possible to extend the experimental tests achievements, considering different driving cycles and regeneration strategies.

IV.2. EXPERIMENTAL RESULTS: SOOT MASS LIMIT TESTS

In this paragraph the main results concerning soot mass limit tests will be discussed. In the first part the temperatures peaks and gradients as a function of the soot loading for the different regeneration procedures will be discussed, while in the second part these data will be compared with the supplier recommendations, in order to assess the agreement between the latter and the experimental tests carried out under the quite severe regeneration tests previously described.

The maximum temperature peaks and temperature gradients measured during a controlled regeneration over the NEDC are shown in Figure IV-1 and Figure IV-2. In these regeneration conditions the exhaust flow helps in expelling the heat generated by the soot combustion, thus limiting the substrate temperature increase. It should be pointed out that, while for Cordierite and Titanate Aluminum the temperature gradient is computed through the entire component, as far as the Silicon Carbide is concerned, the temperature gradient is computed only inside a single segment, since the cement between the segments stops the cracks diffusion. The experimental results highlighted a quite modest or even negligible maximum temperature and thermal gradient increase with increasing soot loadings for both Cordierite and Silicon Carbide. On the contrary, the Aluminum Titanate component showed a strong and clear linear dependency of the maximum temperature with increasing soot loadings. This trend can be explained on the basis of the material properties: Aluminum Titanate has the lowest thermal conductivity between the investigated materials, thus hindering the heat transfer from the hottest zones and leading to a higher sensitivity

of the peak temperatures to the soot loading. On the contrary the higher thermal conductivity of Silicon Carbide and Cordierite seems to compensate for the increase of heat generated by higher burned soot masses, thus leading to an almost negligible peak temperature increase with increasing soot loading. The analysis of the temperature gradients reported in Figure IV-2 clearly shows the effect of the different thermal conductivity: the Silicon Carbide (which has the highest thermal conductivity) shows the lowest temperature gradients, while the Aluminum Titanate (which has the lowest thermal conductivity) shows the highest ones.

The maximum temperature peaks and temperature gradients measured during an uncontrolled regeneration in case of a DTI maneuver are reported in Figure IV-3 and Figure IV-4: comparing these trends with those obtained for the controlled regeneration over the NEDC, clearly highlights that the Drop To Idle represents the worst case condition for the DPF safety, since both peak temperatures and gradients are significantly higher for all the substrates. Again, the Aluminum Titanate component reached the highest temperatures and gradients, while the lowest levels were achieved by the Silicon Carbide thanks to its higher thermal conductivity, with Cordierite showing intermediate values. It is also worth to be noticed that for this kind of uncontrolled regeneration all the materials show clearly increasing trends with increasing soot loading for both the peak temperature and the temperature gradients. In particular data shown in Figure IV-3 highlight that temperature peaks trends of Aluminum Titanate and Silicon Carbide have a similar slope. This can be justified considering that the two substrates have a similar volumetric heat capacity, and, as a consequence, for the same increase in soot loading (and thus in the heat released) the two materials will show a similar temperature increase. However the Aluminum Titanate has a lower thermal conductivity, and this reduces the substrate volume interested by the heat exchange, thus leading to higher temperatures inside the component. The Cordierite has instead a lower volumetric heat capacity, compared to the other substrates, and a lower thermal conductivity than Silicon Carbide, but a higher thermal conductivity than Aluminum Titanate. This results in a trend with a higher slope compared to those of Silicon Carbide and Aluminum Titanate, but with lower peak temperatures if compared to Aluminum Titanate

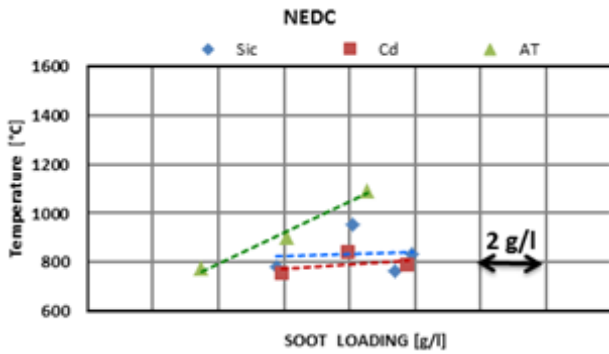


Figure IV-1 Maximum temperature versus soot loading during the RGN event over the NEDC shown in Figure II-6a

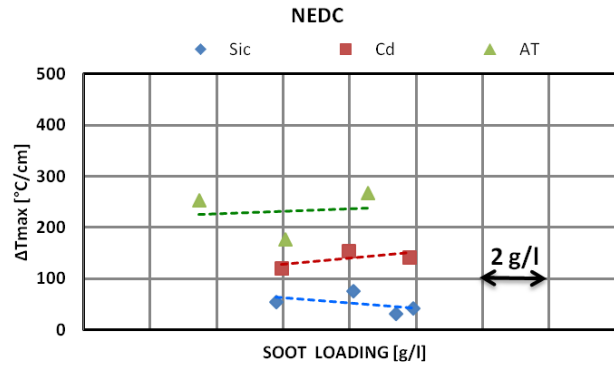


Figure IV-2 Maximum temperature gradient versus soot loading during the RGN event over the NEDC shown in Figure II 6a

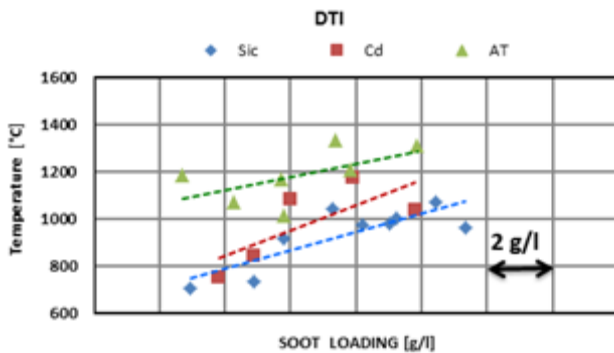


Figure IV-3 Maximum temperature versus soot loading during the DTI RGN event shown in Figure II 6b

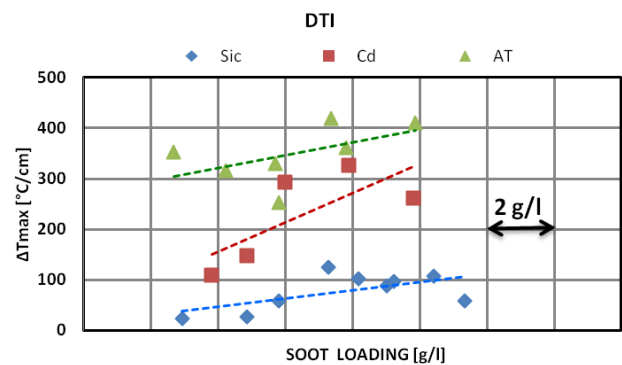


Figure IV-4 Maximum temperature gradient versus soot loading during the DTI RGN event shown in Figure II 6b

Data collected from the regeneration tests were then compared with the suppliers' recommendations or limits.

These limits are usually given in terms of maximum temperature peak and temperature gradient: these two parameters describe the boundaries of a safety area that must not be exceeded. Figure IV-5, Figure IV-6 and Figure IV-7 show the results obtained for the three materials, where the regeneration events that permanently damaged the component are highlighted by a circle. Each filter that did not fulfill any more the Particulate Number or Particulate Matter Euro 6 limits over the NEDC was classified as permanently damaged [31]. It is worth to be recalled that the first limit on PN is the more severe, since also micro cracks that would keep the DPF below the PM mass limit, would not allow fulfilling anymore the PN requirements.

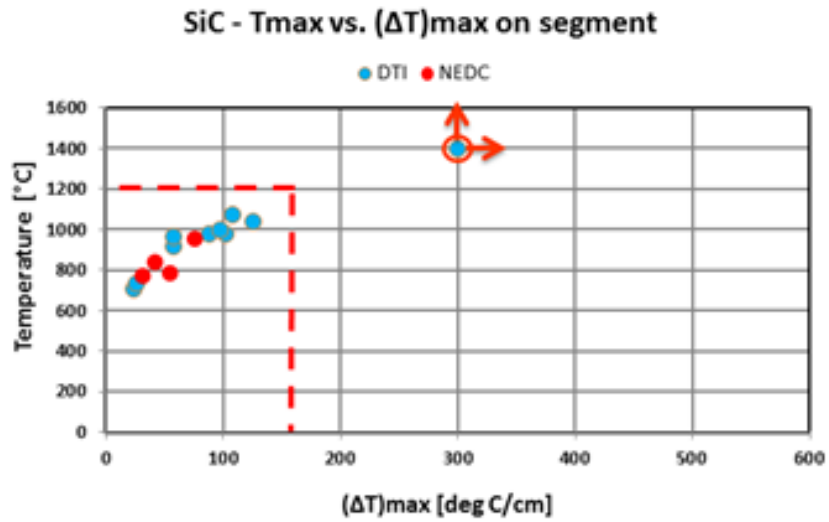


Figure IV-5 Maximum temperature peak versus maximum temperature gradient reached during regenerations for Silicon Carbide

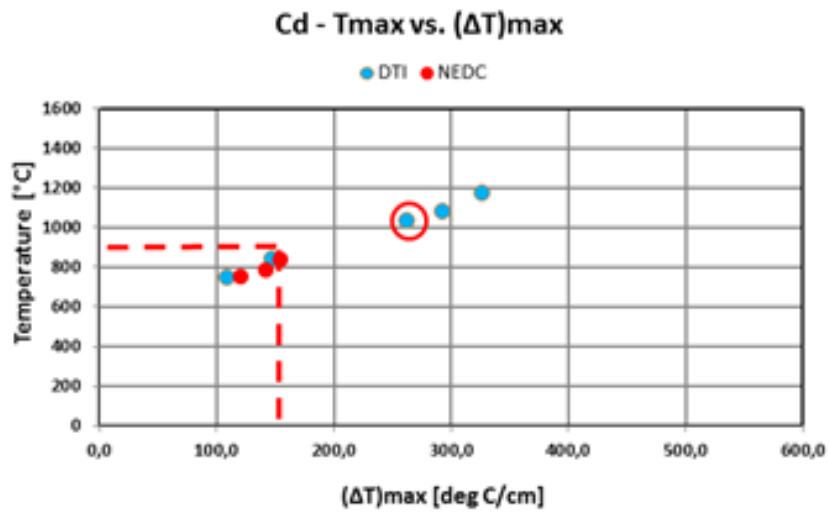


Figure IV-6 Maximum temperature peak versus maximum temperature gradient reached during regenerations for Cordierite

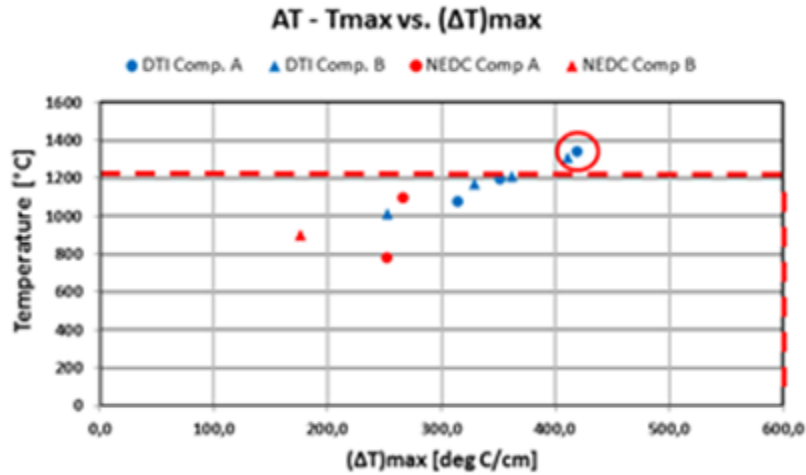


Figure IV-7 Maximum temperature peak versus maximum temperature gradient reached during regenerations for Aluminum Titanate

As far as Silicon Carbide and Aluminum Titanate are concerned, the uncontrolled regeneration which reached the highest temperature was the one that led to the component failure. On the Cordierite component, instead, the emission target was not fulfilled any more after a regeneration that showed lower peak temperatures and gradients compared to the previous ones (with lower soot loadings). The low number of tests performed did not allow to determine if this is an isolated phenomenon or a symptom of a fatigue effect on this material [17]. Another key parameter to be monitored is the regeneration efficiency: a lower efficiency would as a matter of fact lead to a higher regeneration frequency since the filter would start the next loading with a higher residual soot mass. The regeneration efficiency is computed as shown in Equation 7 here below, where soot loading start and soot loading end refers respectively to the soot loading before and after the regeneration event

$$RGN\ Eff. [\%] = \left[\frac{\text{soot loading start} - \text{soot loading end}}{\text{soot loading start}} \right] * 100$$

Equation 7 Regeneration efficiency

Figure IV-8 and Figure IV-9 show the regeneration efficiency as a function of the maximum temperature and of the soot loading, respectively, in case of controlled regenerations over the NEDC. A linear dependency from the soot loading can be clearly noted for Cd and SiC. As far as the AT is concerned, the limited number of experimental

points and their variability does not allow assessing a clear correlation of regeneration efficiency as a function of soot loading and maximum regeneration temperature.

Figure IV-10 and Figure IV-11 represent the regeneration efficiency as a function of maximum temperature and soot loading in case of a drop to idle event. In this case, differently from what was observed in the regenerations over the NEDC, only Silicon Carbide and Cordierite showed linearly increasing trends, while the Aluminum Titanate showed an almost opposite trend. This trend could be justified considering that during a drop to idle regeneration event the lower thermal conductivity of the material does not allow a good regeneration in the external part of the component: the higher is the soot load, the stronger is the effect.

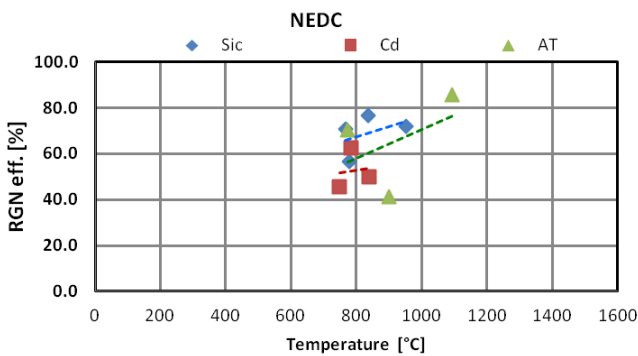


Figure IV-8 Regeneration efficiency as a function of maximum temperature (controlled RGN events during NEDC)

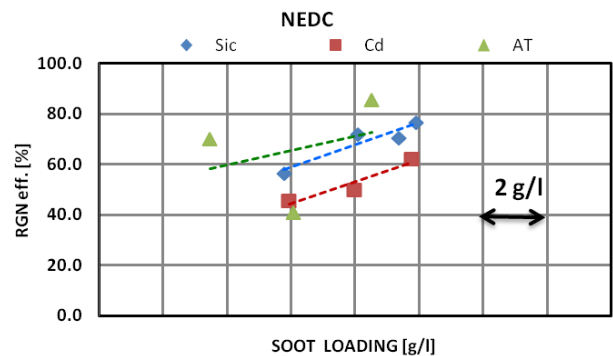


Figure IV-9 Regeneration efficiency as a function of soot loading (controlled RGN events during NEDC)

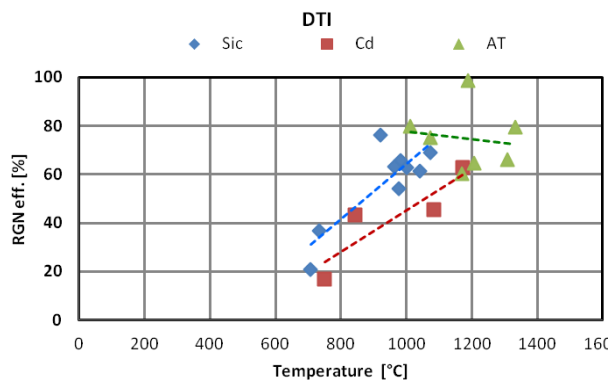


Figure IV-10 Regeneration efficiency as a function of maximum temperature (uncontrolled RGN events during DTI).

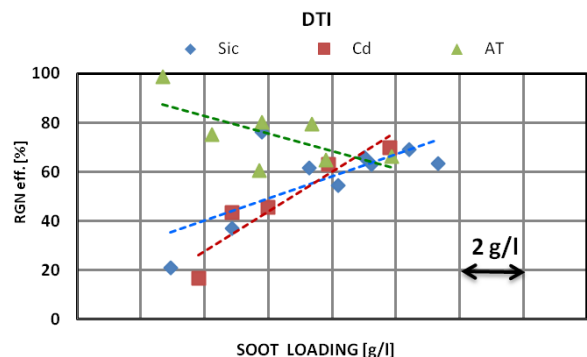


Figure IV-11 Regeneration efficiency as a function of soot loading (uncontrolled RGN events during DTI).

IV.3. DPF REGENERATION MODEL RESULTS

Since the collection of the data summarized in IV.2, requires a considerable experimental effort, a 0D DPF Model (described in III.3) was set-up in order to predict the maximum substrate temperature varying the regeneration parameters and the filter properties.

In order to validate the model, defined soot loadings, not necessarily those corresponding to the experimental tests, were simulated considering both a DTI maneuver both a regeneration over the NEDC cycle. Since the regeneration efficiency is influenced from three-dimensional factors like not uniform temperature distribution inside the filter or local scarcity of oxygen, it cannot be predicted from a 0D regeneration model. For this reason, the linear interpolation of the experimentally measured regeneration efficiency, showed in Figure IV-8 - 11Figure IV-11, was used in order to consider the correct soot mass involved in the regeneration process.

Figure IV-13, Figure IV-14 and Figure IV-15 show the comparison between the model prediction and the experimental data considering the DTI regeneration event. In the pictures the blue rhombuses represent the experimental data, while the red squares show the model prediction: for all the three substrates the model is capable to predict correctly the experimental trend.

Figure IV-16 and Figure IV-18 show, for SiC and Cd respectively, the comparison between the model prediction and the experimental results over a NEDC cycle regeneration. In these two cases the model predicts a trend with a higher slope compared to the experimental data, but in any case with similar maximum temperatures. The main reason for this divergence, has to be attributed to the experimental variability and to the lower number of tests available. Figure IV-17 shows the results for the Aluminum Titanate, in this case, where a stronger correlation between maximum regeneration temperature and soot loading can be observed, the model shows a better predictivity.

Once validated the model was used to evaluate the possible benefits, in terms of maximum substrate temperature reduction, of specific calibration strategies [71], [72], [73], [74], [75] aimed to preserve the filter from a thermal shock reducing the oxygen availability in the exhaust flow by opening the EGR valve.

Figure IV-12 shows as an example the simulated substrate temperature trends in the case of a DTI event in an Aluminum Titanate filter. In this picture the blue lines refer to the drop to idle with the standard engine calibration, while the green lines represent the results

achievable with a specific calibration strategy aimed to the peak temperature reduction. In particular the dashed lines in the bottom of the picture represent the oxygen concentration at the DPF inlet, the dotted lines in the top of the figure show the soot mass trend during the regeneration process, while the continuous lines in the middle of the picture represent the filter substrate temperature and the exhaust mass flow rate.

Looking at the DTI event with the standard calibration, an increase of the oxygen concentration can be noticed as the engine drops to idle; this contributes to increase the soot oxidation rate and consequently the maximum filter substrate temperature reached during the regeneration event.

Opening the EGR, as the engine speed falls to idle, allows instead to reduce the oxygen concentration at exhaust, and consequently the soot oxidation rate in the filter. As a matter of facts, looking at the soot mass trends during the filter regeneration, a remarkable slowdown of the soot combustion rate can be appreciated as the oxygen availability is reduced. As shown by the filter substrate temperature trends, thanks to the lower heat release rate of the soot combustion, a lower maximum temperature in the filter substrate can be achieved.

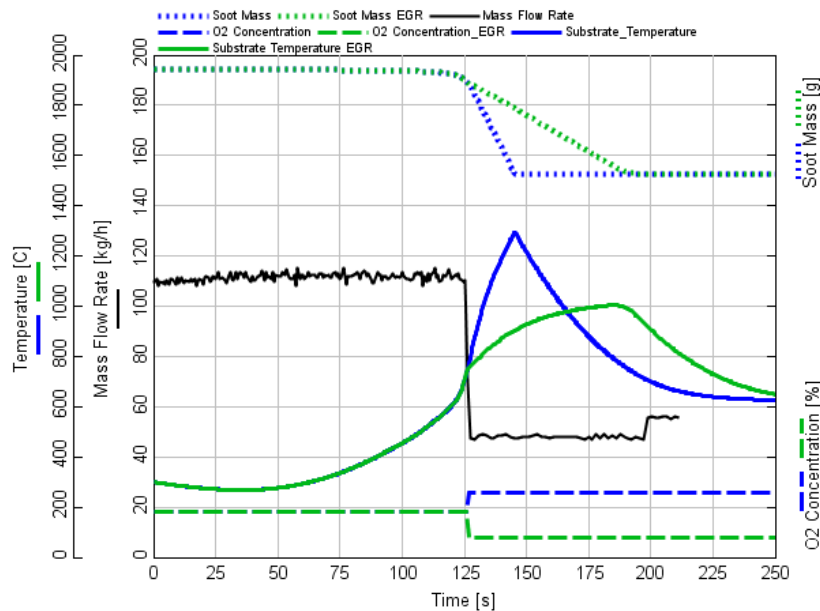


Figure IV-12 Simulation of the Substrate Temperature in an AT DTI event with and without maximum temperature control strategy

The maximum temperatures, predicted from the model, in the case of this specific regeneration strategy were adopted, are reported in Figure IV-13, Figure IV-14 and Figure IV-15 with the green triangles. Looking at the pictures a maximum regeneration temperature reduction ranging from 100 °C up to 200 °C can be observed in all the cases, thus allowing to preserve the component integrity also at high filter soot loadings.

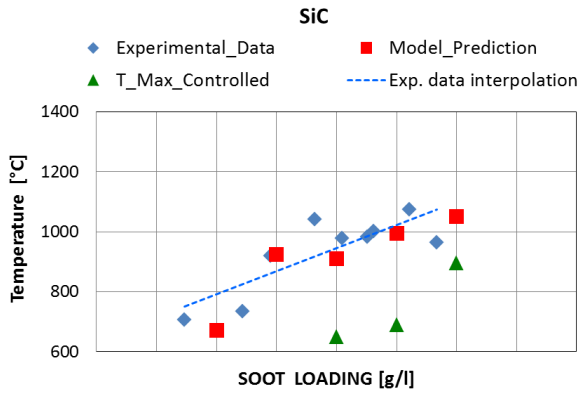


Figure IV-13 Comparison between experimental data and model prediction in case of SiC DTI regeneration event

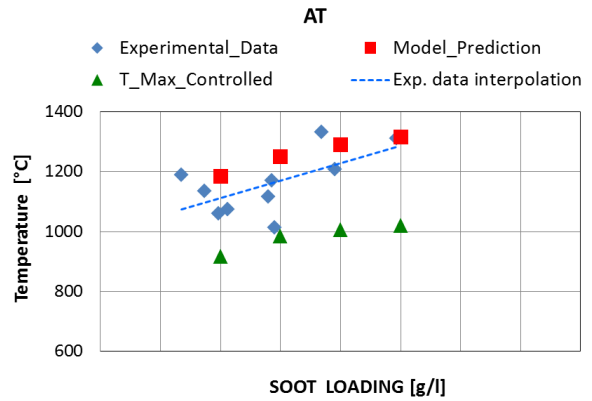


Figure IV-14 Comparison between experimental data and model prediction in case of AT DTI regeneration event

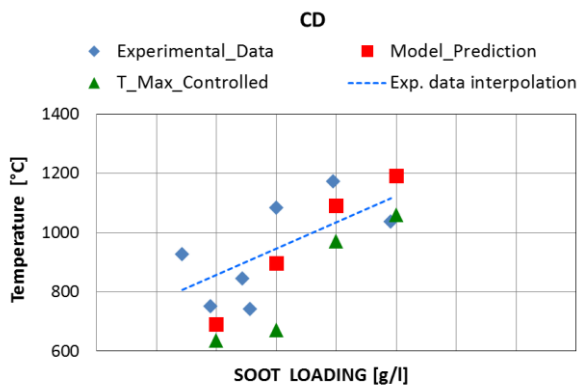


Figure IV-15 Comparison between experimental data and model prediction in case of Cd DTI regeneration event

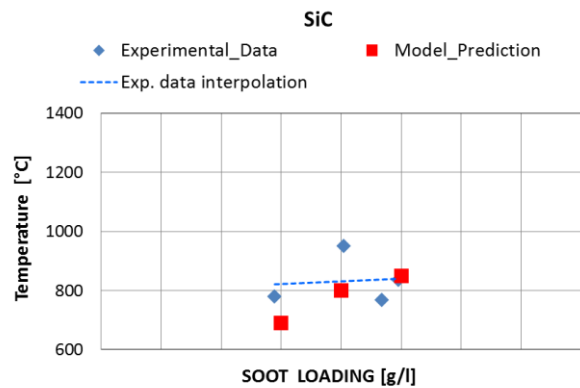


Figure IV-16 Comparison between experimental data and model prediction in case of SiC regeneration over the NEDC cycle

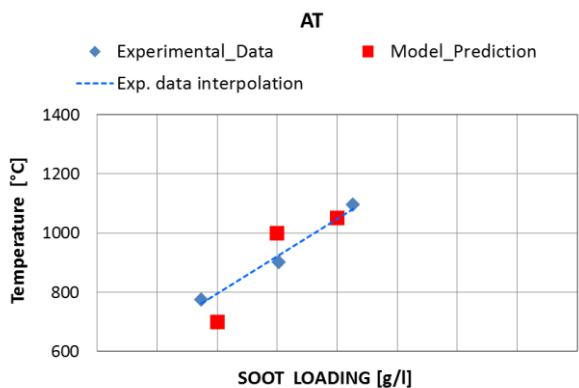


Figure IV-17 Comparison between experimental data and model prediction in case of AT regeneration over the NEDC cycle

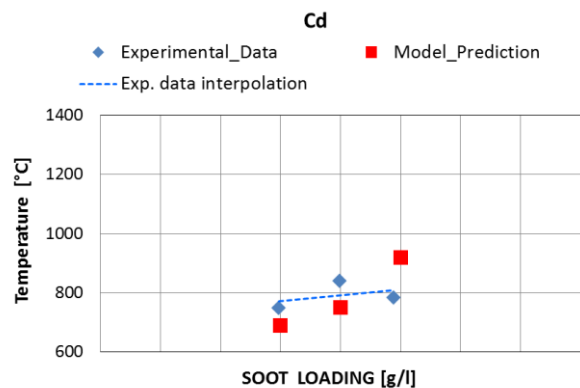


Figure IV-18 Comparison between experimental data and model prediction in case of Cd regeneration over the NEDC cycle

IV.4. SOOT MASS LIMIT IMPACT ON FUEL CONSUMPTION AND OIL DILUTION

It is well known that DPF regeneration requires specific engine strategies with fuel post-injections close to BDC which have clear drawbacks in terms of increased fuel consumption and decreased lube oil life. For a fixed engine and after-treatment layout, the only way to mitigate these drawbacks is to reduce the regeneration frequency. The influence of the different substrates characteristics on the regeneration frequency was therefore evaluated simulating the load and the regeneration of the filters over the four different driving cycles described in the 1-D engine model section, which makes it possible to simulate the system behavior on a large variety of driving conditions.

In order to define, for each substrate, the soot loading at which the filter regeneration should be triggered, referred as soot mass limit (SML), three different hypotheses were considered. The first hypothesis (SML1) considers the introduction of a Safety Coefficient (S.C.) computed on the basis of the SiC results, which were assumed as a benchmark, since SiC was the material that showed the highest soot loading before cracking. As shown in Equation 8 the safety coefficient was calculated by dividing the soot loading at which the SiC component was damaged (experimental soot mass limit) by the soot loading at which a regeneration event is usually triggered (SiC soot mass limit).

$$S.C. = \frac{\textit{experimental soot mass limit}}{\textit{target regeneration soot loading}}$$

Equation 8 Safety Coefficient (S.C.) definition

This safety coefficient was then used to calculate the target soot loading at which a regeneration event should be triggered for Cordierite and Aluminum Titanate, in order to maintain the same safety margin as for Silicon Carbide. As a consequence, for each substrate, the soot mass limit was defined by dividing the soot loading at which the component was permanently damaged by the SiC safety coefficient

The second hypothesis (SML2) considers to regenerate the filter at the experimental soot mass limit, without taking in account any safety coefficient. As discussed in IV.3, this could be possible if specific regeneration strategies, aimed to reduce the temperature peaks in a

DTI event were introduced. In this case, the maximum temperatures and gradients reached would be drastically reduced ensuring the component safety.

Finally a third and last hypothesis (SML2+SCR) considers always to trigger a regeneration at the experimental soot mass limit, but it takes also into account the adoption of a NO_x aftertreatment device placed downstream the DPF (for example an SCR). Even if the regeneration frequency is unchanged, the fuel consumption drawbacks related to the additional backpressure generated by the SCR have to be taken into account.

After defining, for each hypothesis, the soot mass limit of the three substrates, the number of cycles necessary to load the component and trigger the regeneration was estimated.

The normalized number of loading cycles, for the different substrates, is reported in Figure IV-19, Figure IV-20, Figure IV-21, Figure IV-22. These pictures report only the first two hypothesis (SML1 and SML2) since the regeneration frequency is not influenced by the eventual SCR adoption. The Silicon Carbide, thanks its higher soot mass limit, is characterized by a much smaller regeneration frequency. The Aluminum Titanate, although presenting a soot mass limit similar to Cordierite, has a smaller regeneration frequency thanks to its higher regeneration efficiency. These results also point out the potentialities, in the regeneration frequency reduction, of the temperature control strategies under a DTI event (SML2 hypothesis). As a matter of fact, the soot mass limit increase allows to cover a more than double distance between two regeneration events.

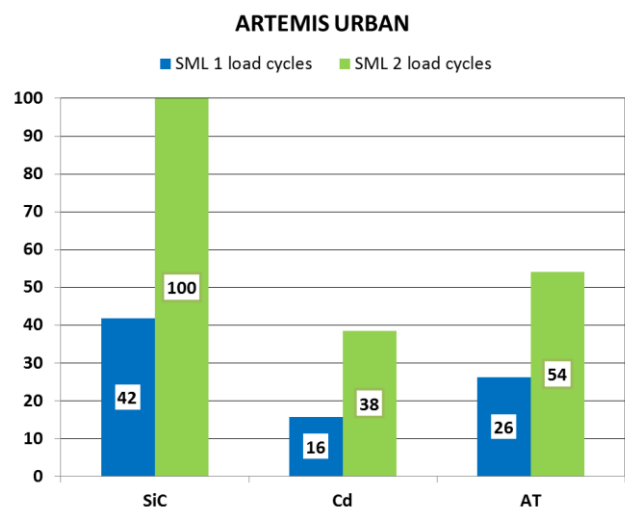
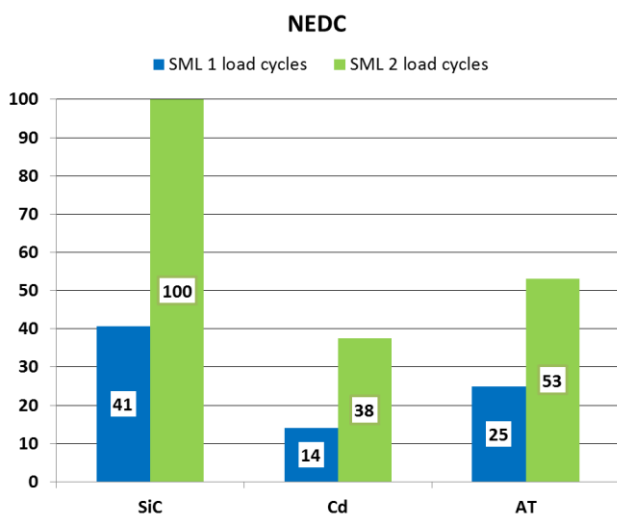


Figure IV-19 Number of NEDC cycles needed to load the component to trigger a regeneration normalized to

Figure IV-20 Number of Artemis Urban cycles needed to load the component to trigger a regeneration

Silicon Carbide (SML2 hypothesis) values

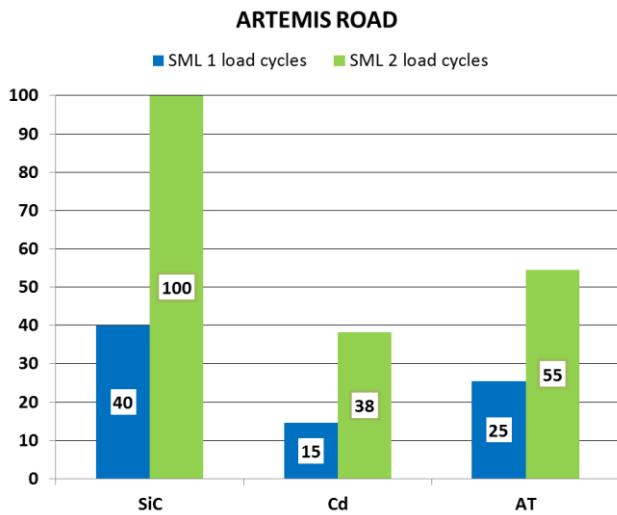


Figure IV-21 Number of Artemis Road cycles needed to load the component to trigger a regeneration normalized to Silicon Carbide (SML2 hypothesis) values

normalized to Silicon Carbide (SML2 hypothesis) values

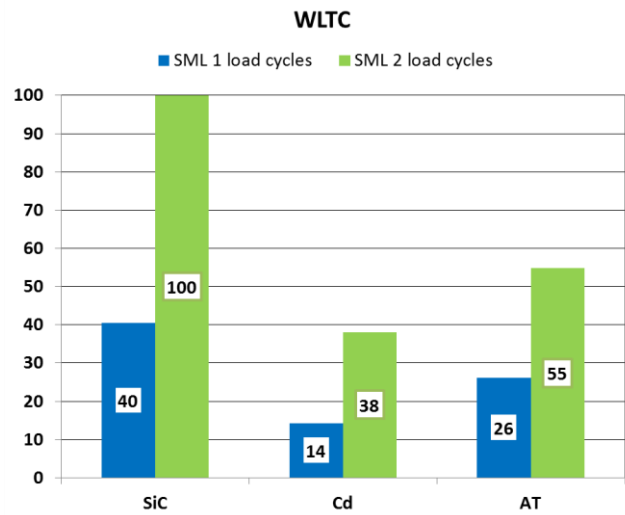


Figure IV-22 Number of WLTC cycles needed to load the component so to trigger a regeneration normalized to Silicon Carbide (SML2 hypothesis) values

On the basis of the results of Figure IV-19, Figure IV-20, Figure IV-21, Figure IV-22, and considering the fuel consumption increment as a function of backpressure showed in Table III.1, the impact of the different materials soot mass limits on the fuel consumption was estimated as shown in Equation 9. In Equation 9 i_{SMLx} represents the number of cycles to reach the target regeneration soot loading, while $FC_{cycle}(i)$ takes into account the fuel consumption increment as a function of backpressure.

$$FC \left[\frac{l}{100 \text{ km}} \right] = \left(\frac{\sum_{i=1}^{i_{SMLx}} FC_{cycle}(i)[l] + FC_{cycle \text{ RGN}}[l]}{\text{Total distance [km]}} \right) * 100$$

Equation 9 RGN impact on Fuel Consumption

The results obtained are reported in Table IV.1 and Table IV.2. Table IV.1 shows the fuel consumption percentage increments, compared to SiC values, for each SML hypothesis. Table IV.2 shows instead, for each substrate, the percentage of fuel consumption savings, in the case of SML2 and SML2+SCR hypothesis, compared to SML1 values.

Considering the SiC results, fuel consumption savings, ranging from 0,8% in the Artemis Urban to 1,6% in the WLTC, can be achieved increasing the target regeneration soot loading (SML2 hypothesis).

Looking at the AT results, as far as the SML1 hypothesis is concerned, the higher regeneration frequency leads to a fuel consumption increment, in all the cycles, of about 1% compared to SiC. Considering the SML2 hypothesis an approximately 2% fuel consumption saving, compared to SML1, can be achieved. Moreover the gap between SiC and AT results is almost canceled: as a matter of facts in this case the fuel consumption increase compared to SiC is lower than 0,6% in almost all the cycles.

The Cordierite was the substrate characterized by the highest regeneration frequencies, and consequently showed the highest fuel consumption increase: from +2.4% in the Artemis Urban up to +4,8% in the WLTC. Considering the SML2 hypothesis, the Cd showed the highest percentage fuel consumption reductions: up to -4% on the WLTC. This high fuel consumption reduction can be explained considering the low Cd soot mass limit: which leads to a higher weight of the regeneration cycle on the total fuel consumption, and consequently to a higher fuel consumption decrease when the loading cycles number is increased. Even if a reduction of Cordierite fuel consumption increase compared to SiC can be observed considering the SML2 hypothesis, increments up to +2% can still be observed.

Taking into account the possible integration with an SCR system, the fuel consumption savings are maintained almost unchanged in all the cycles except the WLTC. In particular, over this cycle, the increased backpressure leads to a fuel consumption penalizations of about +1.3% for all the substrates. Looking in particular at the SiC results, it is worth to note how this makes almost vain the fuel consumption savings generated by the higher regeneration soot loading.

	SML1		SML2		SML2 + SCR	
	Cd	AT	Cd	AT	Cd	AT
NEDC	3,62%	1,13%	1,42%	0,64%	1,42%	0,64%
Artemis Urban	2,39%	0,75%	0,95%	0,38%	0,95%	0,38%
Artemis Road	3,85%	1,17%	1,58%	0,66%	1,58%	0,66%
WLTC	4,79%	1,06%	1,94%	0,47%	1,94%	0,47%

Table IV.1 Fuel consumption increment compared to SiC for each soot mass limit hypothesis

	SML2			SML2 + SCR		
	SiC	Cd	AT	SiC	Cd	AT
NEDC	-1,20%	-3,30%	-1,68%	-0,85%	-2,96%	-1,35%
Artemis Urban	-0,80%	-2,19%	-1,16%	-0,51%	-1,91%	-0,88%
Artemis Road	-1,40%	-3,56%	-1,90%	-1,02%	-3,18%	-1,51%
WLTC	-1,58%	-4,25%	-2,16%	-0,29%	-3,01%	-0,88%

Table IV.2 Fuel consumption reduction for each substrate respect the SML1 hypothesis

The second drawback of an increased regeneration frequency is related to oil life reduction. Starting from the known data of the current Euro 5 engines, the influence of the different regeneration frequencies on oil life was also evaluated over the Artemis Urban cycle, that represent the most critical condition for the oil dilution effect. As a matter of facts the low engine speeds and loads require stronger post injection strategies in order to raise the exhaust temperature up to 600 °C. Figure IV-23 shows the main results: in particular the percentage oil life increase compared to the same material SML1 hypothesis is highlighted in blue, while the oil life percentage reduction compared to SiC values with the same soot mass limit hypothesis is highlighted in red. The picture reports only the values of the SML1 and SML2 hypothesis, because, as already discussed, the adoption of a NO_x aftertreatment system placed downstream the DPF does not give any influence on regeneration frequency and consequently on oil life. Looking at the SML1 hypothesis results, oil life reductions form -36% for AT up to -60% for Cordierite can be noticed. By decreasing the regeneration frequency (SML2 hypothesis), a more than double oil life can be achieved, however the gap between the SiC and the other substrates is maintained almost unchanged.

ARTEMIS URBAN

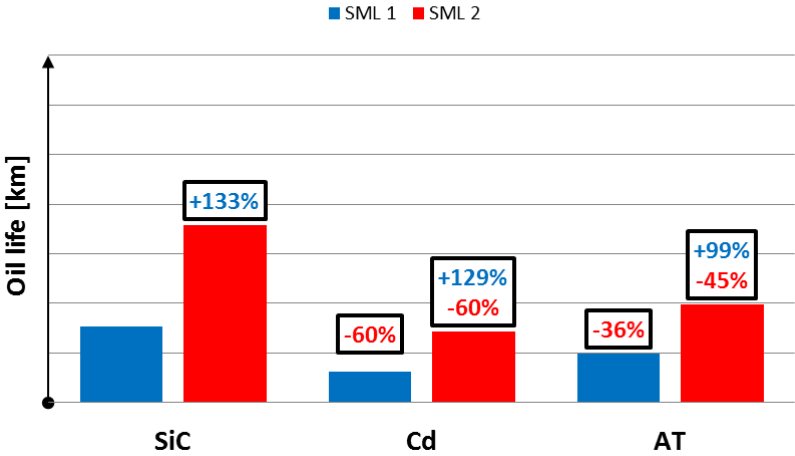


Figure IV-23 Influence of regeneration frequency on the oil life over the Artemis Urban

CHAPTER V. ANALYSIS OF SULPHUR POISONING EFFECT ON DOC CONVERSION EFFICIENCY

V.1. INTRODUCTION

In the first part the performance characterization of cc(DOC+DPF) is evaluated as a function of sulfur poisoning and the effectiveness of de-sulfation process is analyzed. Afterwards, the light-off curves considering different space velocities are discussed.

V.2. CC(DOC+DPF) PERFORMANCE CHARACTERIZATION

In this section, the emission characteristics of CO, HC and NO_x are discussed over and during different stages of NEDC.

V.2.1. Degreened vs. poisoned

The overall CO abatement efficiency over DOC and DOC+DPF is depicted in Figure V-1. DOC showed a continuous loss of performance after each poisoning procedure which is not linear with respect to accumulated sulfur quantity. A decrease of about 50% between degreened and the case with sulfur poisoned of 3.58 gr/l was observed. On the other hand, DPF led to an increase of efficiencies. Lightly sulfur poisoned system (0.36 gr/l) exhibited efficiencies which were similar to the one detected with degreened system. DPF+DOC system seemed to reach steady state poisoning level due to a kind of saturation.

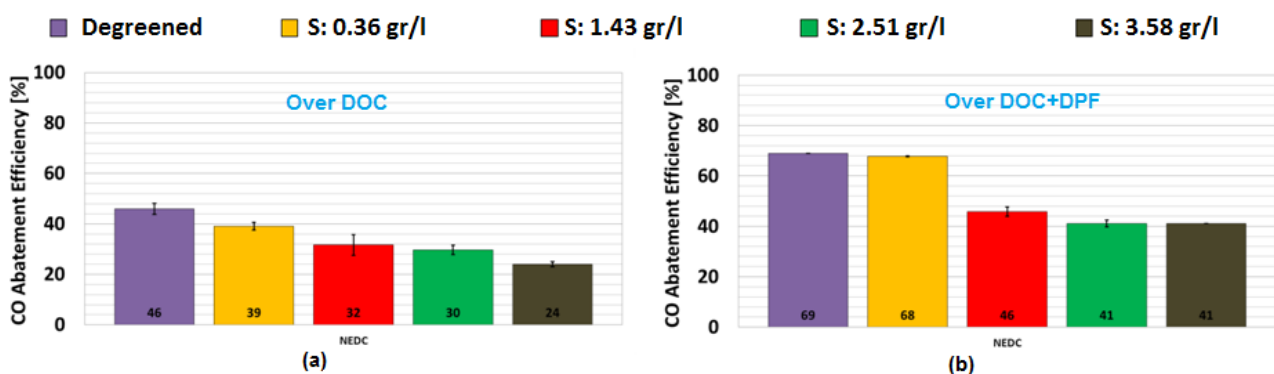


Figure V-1 NEDC global analysis for CO emissions for different poisoning levels; (a) CO abatement efficiency over DOC, (b) CO abatement efficiency over DOC+DPF

The performance of the system regarding CO reduction over different stages of NEDC is shown in Figure V-2. Degreened system showed the highest efficiency. Only degreened system reached light-off temperature during urban portion of NEDC, Figure V-2. Poisoning affected systems efficiency even when a small quantity of sulfur was accumulated on DOC (0.36 gr/l). DPF led to an increase of efficiencies with respect to over DOC efficiencies and recovered the efficiency gap highlighted over DOC only for the 0.36 gr/l system.

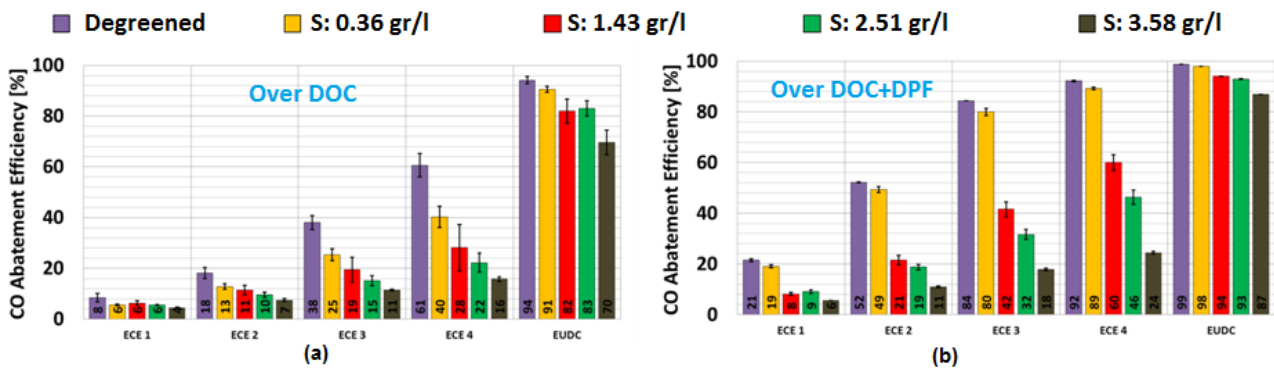


Figure V-2- NEDC breakdown analysis for CO emissions for different poisoning levels; (a) CO abatement efficiency over DOC, (b) CO abatement efficiency over DOC+DPF

HC presented similar trend to CO performance with poisoning as it is apparent in Figure V-3. A decrease of 55% of HC abatement efficiency for 3.58 gr/l vs. degreened was noted. Lightly sulfur poisoned system (0.36 gr/l) exhibited efficiencies which were similar to the one detected with degreened system over DOC+DPF.

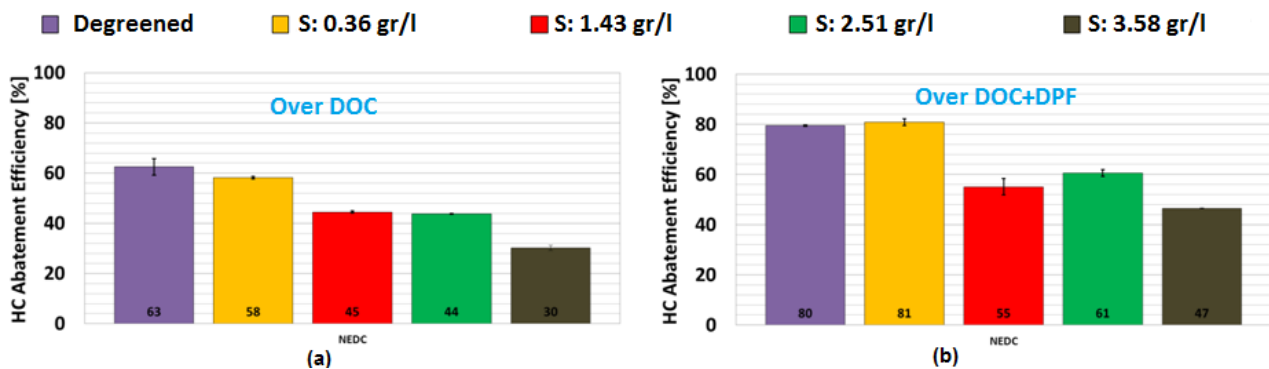


Figure V-3- NEDC global analysis for HC emissions for different poisoning levels; (a) HC abatement efficiency over DOC, (b) HC abatement efficiency over DOC+DPF

As it is apparent in Figure V-4, during NEDC the HC efficiencies over DOC initially were high, then reached a minimum and finally increased. Minimum level of efficiency was

reached in delay (ECE3) for poisoned systems compared to degreened system (ECE2). In this part also the DPF could recover the gap in the low sulfur poisoned case.

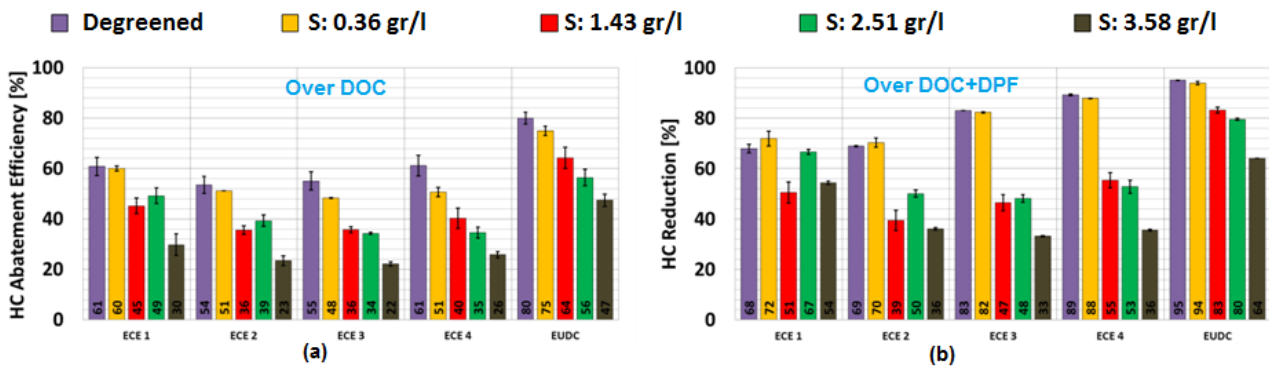


Figure V-4- NEDC breakdown analysis for HC emissions for different poisoning levels; (a) HC abatement efficiency over DOC, (b) HC abatement efficiency over DOC+DPF

The decay trend of CO and HC efficiencies as a function of sulfur poisoning level is illustrated in Figure V-5. It can be noticed that the decrease in efficiency over DOC specially is continuous, while through DPF after a certain value it reaches a steady level of poisoning in which the major part of active sites are poisoned. It is worth mentioning that the case with 1.43 gr/l of sulfur has a wide band of uncertainty which can be observed in Figure V-3, which can be due to measurement errors.

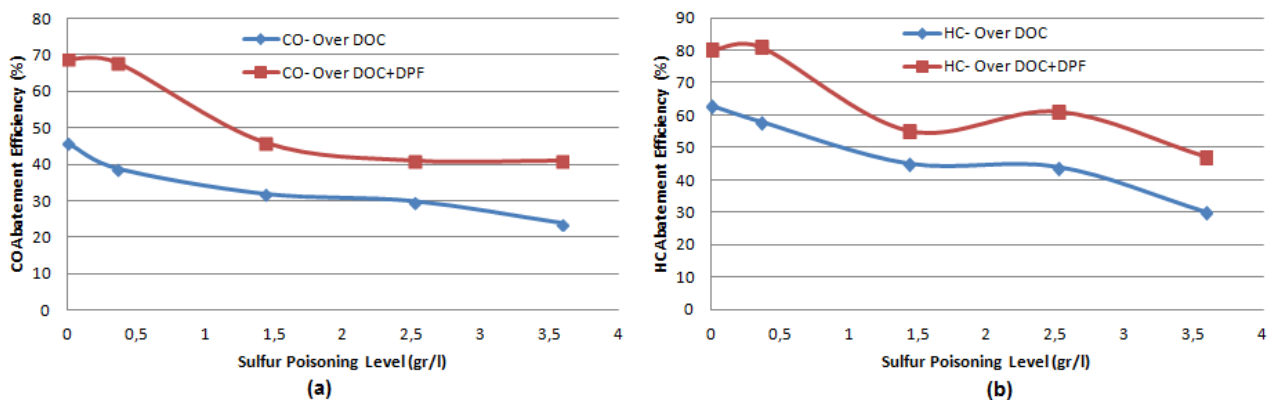


Figure V-5- Abatement efficiency over DOC and DOC+DPF as a function of poisoning level; (a) CO, (b) HC

The temperature profile downstream of DOC and DPF is shown in Figure V-6. It can be observed that heavily poisoned components exhibited lower temperature downstream of DOC.

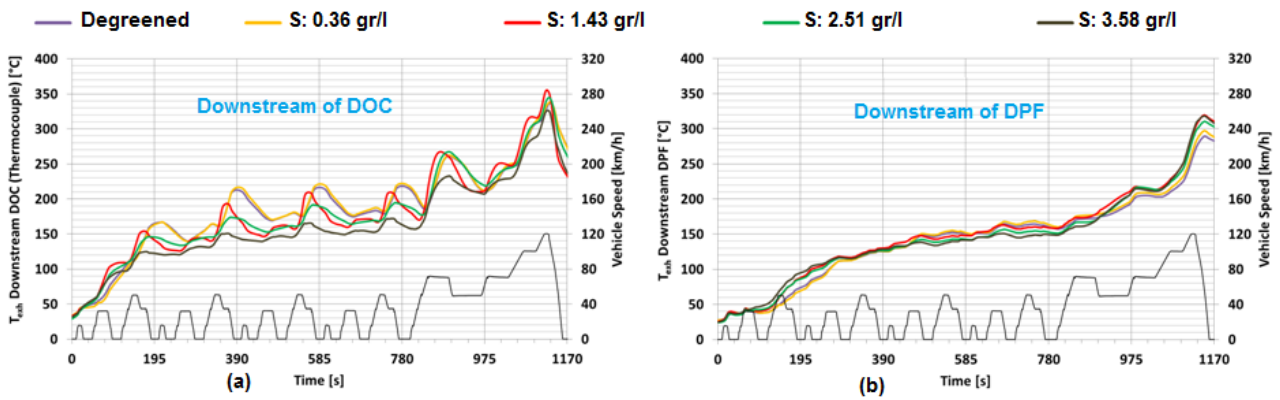


Figure V-6-Temperature profile during NEDC for different poisoning levels; (a) downstream of DOC, (b) downstream of DPF

V.2.2. Recovery of efficiency after de-sulfation compared to degreened

With the aid of proper de-sulfation strategy, it can be observed in Figure V-7 that after de-sulfation over DOC the CO abatement efficiency was recovered completely. In addition, DPF significantly contributed to an increase of abatement efficiencies. Desulfated exhaust systems fully recovered CO abatement efficiency with the only exception of desulfated @ 0.36 gr/l cc(DOC+DPF).

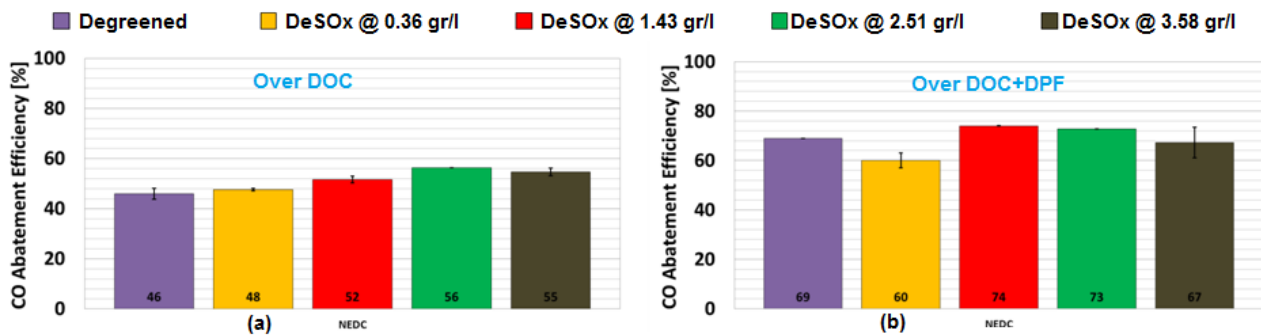


Figure V-7- NEDC global analysis for CO emissions for different de-sulfation levels; (a) CO abatement efficiency over DOC, (b) CO abatement efficiency over DOC+DPF

The overall HC abatement efficiency over DOC, depicted in Figure V-8, for the systems after de-sulfation, with the only exception of DeSOx @ 1.43 gr/l, was recovered completely. DeSOx @ 1.43 gr/l exhibited a lower abatement efficiency which is in good agreement with the light-off curves tests. DPF contributed to an increase of abatement efficiency.

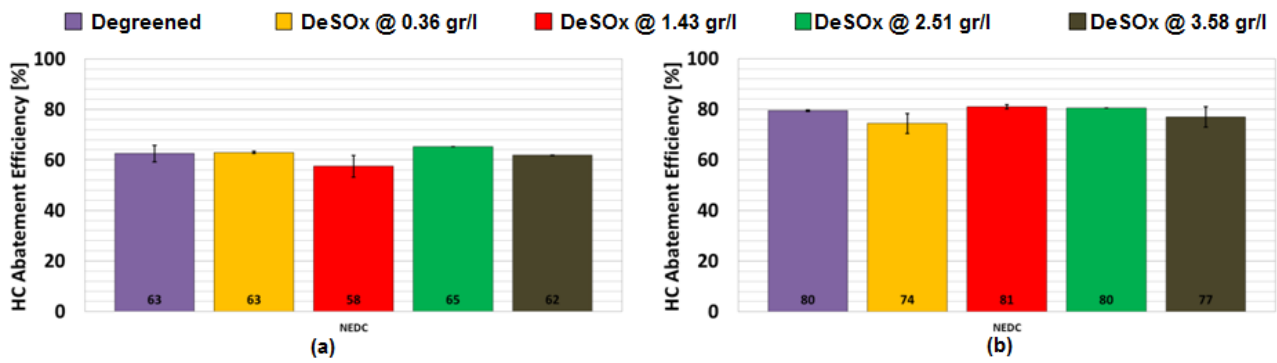


Figure V-8- NEDC global analysis for HC emissions for different de-sulfation levels; (a) HC abatement efficiency over DOC, (b) HC abatement efficiency over DOC+DPF

Comparable temperature profiles were observed for Degreend and DeSOx systems as available in Figure V-9.

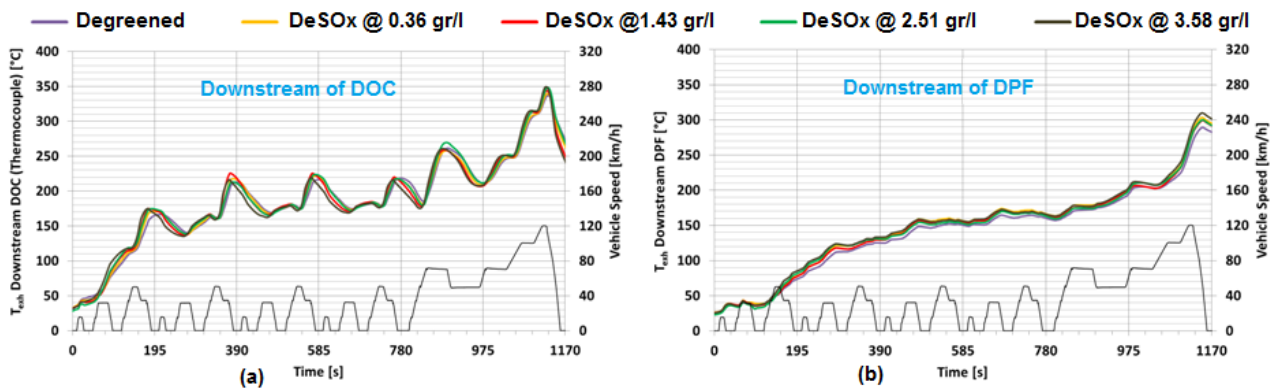


Figure V-9- Temperature profile during NEDC for different de-sulfation levels; (a) downstream of DOC, (b) downstream of DPF

V.3. CC(DOC+DPF) LIGHT-OFF CURVES

The light-off curves are obtained through a transient ramp cycle described in section II.3.2.4 (Figure II-8) for the operating points listed in Table II.8 and considering degreened, poisoned and de-sulfated exhaust systems.

The effect of space velocity on CO and HC light-off curve in the case of degreened system is depicted in Figure V-10. It is apparent that different space velocities did not affect the CO maximum efficiency which was achieved during tests, nor the light off temperature. On the contrary, different minimum and maximum HC abatement efficiencies in addition to various maximum exhaust gas temperature was observed. It is worth mentioning that significant changes in the cool down phase for both HC and CO can be noticed.

It is noteworthy that the initial decay of HC performance in light-off curve is attributed to adsorption of HC at low temperatures, due to trapping effect of Zeolite, and its release at higher temperatures. Moreover, details about light-off temperature and the hysteresis effect observed in light-off curves were explained in section II.3.2.4..

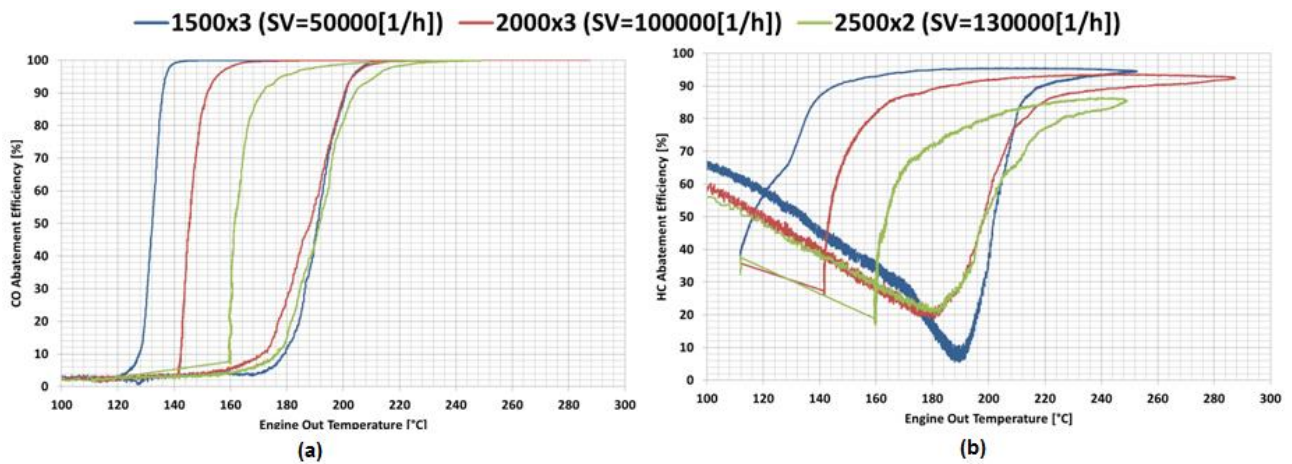


Figure V-10- Light-off curve of degreened system for different space velocities; (a) CO, (b) HC

Among the experiments performed on poisoned systems, highly poisoned (3.58 gr/l) is illustrated in Figure V-11. As it can be observed, space velocity affects the CO maximum efficiency which was achieved during tests, such that the highest space velocity exhibited the lowest maximum efficiency. The trend of HC light-off curve in the poisoned case is similar to the degreened one with different maximum temperatures. Moreover, the lowest space velocity showed the lowest minimum and highest maximum HC abatement efficiency. Space velocity highly affects the poisoned system.

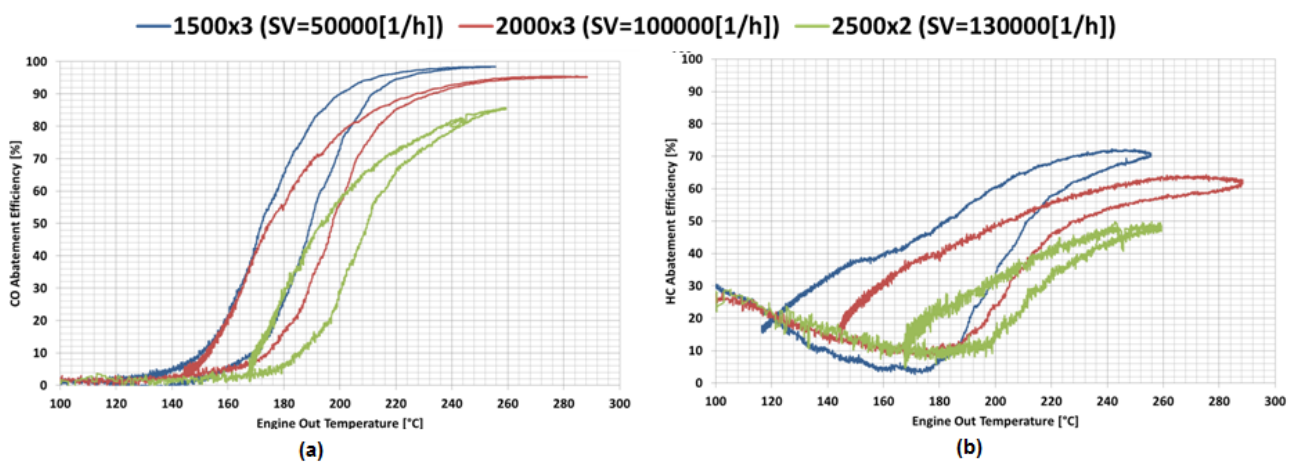


Figure V-11- Light-off curve of 3.58 gr/l sulfur (highly poisoned) system for different space velocities; (a) CO, (b) HC

Finally, an example of light-off curve for de-sulfated systems is shown in Figure V-12, DeSOx @ 3.58 gr/l. The results obtained in de-sulfated systems for both HC and CO light-off are almost similar to the degreened catalyst except that the light-off temperature is also affected; as shown in Figure V-13, a variation of about 10°C in light off temperature for the highest space velocity is observed with respect to other space velocities. It is apparent that although overall performance of de-sulfation over global NEDC is comparable to degreened system as depicted in Figure V-7 and Figure V-8, variation of space velocity influences that performance of de-sulfated system regarding CO light-off curve, while in the degreened case the light-off curve remained unchanged for different values of space velocities.

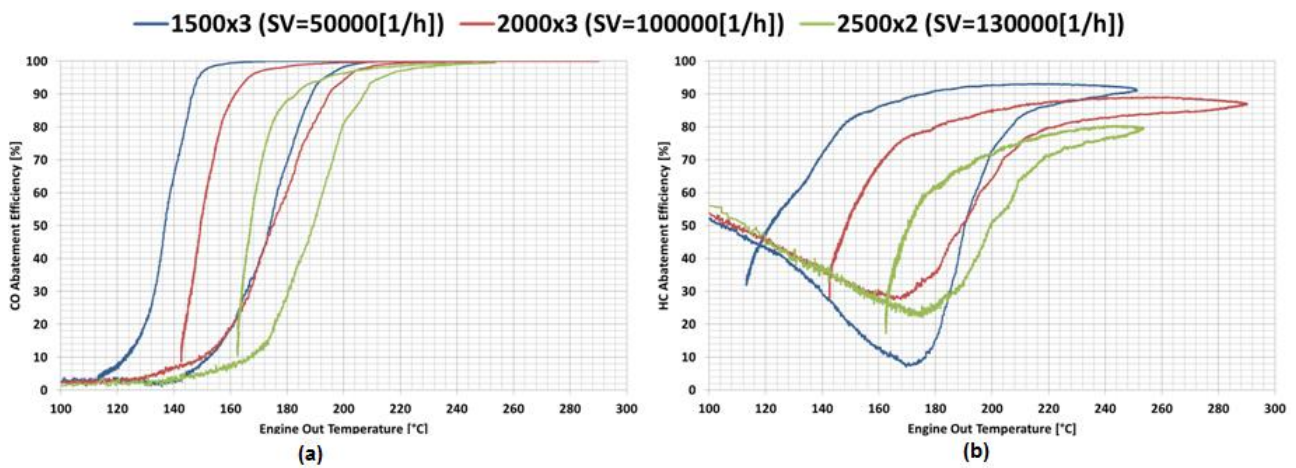


Figure V-12- Light-off curve of DeSOx @ 3.58 gr/l system for different space velocities; (a) CO, (b) HC

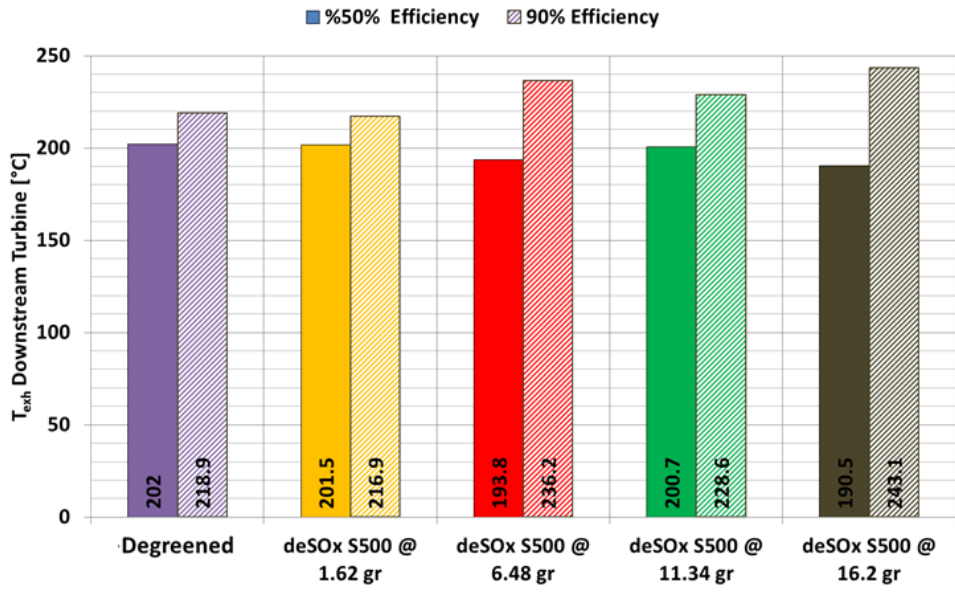


Figure V-13 Light-Off temperature comparison degreened vs DeSOx

Conclusions

In this work an experimental and numerical investigation of a closed coupled DOC-DPF system for automotive application was performed considering the integration with other after-treatment systems and the impact of the usage of different fuels.

First, the influence on fuel consumption and oil dilution of three different substrate materials (Silicon Carbide, Cordierite and Aluminum Titanate) was investigated. The filters were soot loaded under real world operating conditions on the road and then regenerated in two different ways that simulate the urban driving conditions, which are the most severe for DPF regeneration, since the low exhaust flow has a limited capability to absorb the heat generated by the soot combustion. A 1-D engine model was then developed in order to predict the fuel consumption increment as a function of the exhaust back pressure caused by the DPF soot loading over different driving conditions. Furthermore a 0-D DPF model was built in order to predict maximum substrate temperature varying the material properties and the regeneration conditions.

The simulation results showed that, except for the high engine speed and high load operating conditions, such as those corresponding to the Extra-High phase of the WLTC driving cycle, the fuel consumption increments caused by the exhaust back pressure increase due to soot loadings were not significant. Consequently the highest soot loading level before DPF regeneration which still ensures the component integrity under an uncontrolled regeneration results in the lowest fuel consumption.

The results showed that Aluminum Titanate and Cordierite, compared to Silicon Carbide, can give significant advantages in reducing the temperature loss across the DPF, thus guaranteeing a better integration with a downstream SCR system.

On the other hand, Aluminum Titanate and Cordierite physical properties lead to smaller soot mass limits under uncontrolled regeneration. The resulting increased regeneration frequency leads to significant penalties in terms of fuel consumption and oil life compared to SiC. However, this gap could be partially recovered by adopting specific regeneration strategies, with the aim of the reduction of maximum temperature under uncontrolled regenerations.

In the second part of the work, the impact of high sulfur fuel on catalyst performance through different stages of poisoning was investigated experimentally on an engine test bench. As expected, increasing the poisoning level results in continuous loss of HC and CO abatement efficiency over DOC, while DPF was capable to recover the efficiency gap highlighted over DOC for lightly poisoned cases. Additionally, only degreened system reached light-off temperature during urban portion of NEDC. It is worth mentioning that by adopting a proper de-sulfation strategy it was possible to recover almost completely the performance of the after-treatment systems with similar results for HC and CO emissions over DOC and DPF..

As a final point, light-off curves were evaluated for degreened, poisoned and de-sulfated systems for different operating conditions considering variable space velocities. In all the cases, significant changes in the cool down phase and maximum exhaust gas temperature for both HC and CO were monitored, in addition to diverse minimum and maximum HC abatement as a function of space velocity. It is worth mentioning that for the degreened system the warm up phase was not affected by space velocity, while in the poisoned systems the influence of space velocity in all stages could be observed.

Bibliography:

- [1] 2008/692/EC, *Implementing and amending Regulation (EC) N. 715/2007 of the European Parliament and of the Council on type-approval of motor vehicles with respect to emissions from light passenger and commercial vehicles (Euro 5 and Euro 6).*, 2008.
- [2] E. E. Agency, «Monitoring CO2 emissions from passenger cars and vans in 2013,» No 19/2014.
- [3] CARB, «http://www.arb.ca.gov/msprog/clean_cars/acc%20summary-final.pdf,» [Online].
- [4] T. Johnson, «Diesel Emission Control in Review,» *SAE International Journal of Fuels and*, vol. 02, n. 01, pp. 1-12, 2009.
- [5] F. Eichler, J. Kahrstedt, M. Köhne, A. Krause e M. De Graaff, «The New 2.0l 4-Cylinder BiTurbo TDI® Engine from Volkswagen,» in *23rd Aachen Colloquium Automobile and Engine Technology 2014*, Aachen, 2014.
- [6] N. Möller, M. Fleiss, A. Olofsson e J. Korsgren, «The New 2.0-L Diesel Engine for the All-New Volvo XC90,» in *23rd Aachen Colloquium Automobile and Engine Technology 2014*, Aachen, 2014.
- [7] T. Köerfer, «The Future Power Density of HSDI Diesel Engines with Lowest Engine out Emissions – A Key Element for Upcoming CO2 Demands,» in *FISITA Conference*, Munich, 2008.
- [8] F. Millo, P. Ferrero Giacominetto e M. Gianoglio Bernardi, «Analysis of different exhaust gas recirculation architectures for passenger car Diesel engines,» *Applied*

Energy, vol. 98, pp. 79-91, 2012.

- [9] Y. Kim, C. Park, J. Kim e B. Min, «The Effect of Low Temperature EGR and Low Compression Ratio on NO_x Reduction for EU6 Diesel Engine,» *SAE Technical Paper*, n. 2013-01-2644, 2013.
- [10] D. Heuwwetter, W. Glewen, D. Foster, R. Krieger e M. Andrie, «Experimental Investigation of Transient Response and Turbocharger Coupling for High and Low Pressure EGR Systems,» *SAE Technical Paper*, n. 2014-01-1367, 2014.
- [11] A. Mehrotra, S. Juttu, S. Ravishankar, G. Rambhaji e J. Suryawanshi, «Simultaneous Reduction of NO_x and PM Emissions through Low Temperature EGR Cooling in Diesel Engines,» *SAE Technical Paper*, n. 2014-01-2803, 2014.
- [12] D. Zeh, J. Hammer, C. Uhr, M. Rückle, A. Rettich, B. Grotta, W. Stöcklein, J. Gerhardt, D. Naber e M. Raff, «Bosch Diesel Injection Technology – Response for Every Vehicle Class,» in *23rd Aachen Colloquium Automobile and Engine Technology 2014*, Aachen, 2014.
- [13] D. Schöppe, F. Atzler, O. Kastner e F. Kapphan, «High Performance Diesel Direct Driven Piezo Common Rail Injection System,» in *23rd Aachen Colloquium Automobile and Engine Technology 2014*, Aachen, 2014.
- [14] T. Tomoda, H. Ohki, T. Koyama e K. Fujiwara, «Study of Diesel Combustion Improvement for Ultra Low Compression Ratio,» in *19th Aachener Kolloquium Fahrzeug- und Motortechnik 2010*, Aachen, 2010.
- [15] T. Sakono, E. Nakai, M. Kataola, H. Takamatsu e Y. Terazawa, «Mazda SKYACTIV-D 2.2L Diesel Engine,» in *20th Aachener Kolloquium Fahrzeug und Motortechnik 2010*, Aachen, 2010.

- [16] F. Tao, Y. Liu, B. H. Rempelwert, D. E. Foster, R. D. Reitz, D. Choi e P. Miles, «Modeling the effects of EGR and injection pressure on soot formation in a high-speed direct-injection,» *SAE Technical Paper*, n. 2005-01-0121, 2005.
- [17] C. J. Mueller e A. Upatnieks, «Dilute clean diesel combustion achieves low emissions and high,» in *11th Diesel Engine Emissions Reduction Conference*, Chicago, 2005.
- [18] A. Bhave, M. Kraft, L. Montorisi e F. Mauss, «Sources of CO emissions in an HCCI engine: A numerical analysis,» *Combustion and Flame*, n. 144, pp. 634-641, 2006.
- [19] S. Imtenan, M. Varman, H. H. Masjuki, M. A. Kalam, H. Sajjad, M. I. Arbab e I. M. Rizwanul Fattah, «Impact of low temperature combustion attaining strategies on diesel engine emissions for diesel and biodiesels: A review,» *Energy Conversion and Management*, n. 80, pp. 329-356, 2014.
- [20] S. Lee, J. Jang, S. Oh, Y. Lee, J. Kim e K. Lee, «Comparative Study on Effect of Intake Pressure on Diesel and Biodiesel Low Temperature Combustion Characteristics in a Compression Ignition Engine,» n. 2013-01-2533, 2013.
- [21] Y. Chao, W. Jian-xin, W. Zhi e S. Shi-jin, «Comparative study on Gasoline Homogeneous Charge Induced Ignition (HCCI) by diesel and Gasoline/Diesel Blend Fuels (GDBF) combustion,» *Fuel*, n. 106, pp. 470-477, 2013.
- [22] Dieselnet, «Dieselnet Technology Guide,» 2014. [Online]. Available: <https://www.dieselnet.com/tg.php#filter>.
- [23] A. Boubnov, S. Dahl, E. Johnson, A. P. Molina, F. M. C. Simonsen, S. Helveg, L. J. Lemus-Yegres e J.-D. Grunwaldt, «Structure–activity relationships of Pt/Al₂O₃ catalysts for CO and NO oxidation at diesel exhaust conditions,» *Applied Catalysis B: Environmental*, n. 126, p. 315– 325, 2012.

- [24] S. Katare, «Aged DOC Is a Net Consumer of NO₂: Analyses of Vehicle, Engine-,» *SAE Technical Paper*, n. 2007-01-3984, 2007.
- [25] H. NOACK, «What impacts the efficiency of SCR-catalyst systems?,» in *Car Training Institute SCR Forum*, Karlsruhe, 2007.
- [26] P. Spurk, S. Frantz, F. W. Schütze e H. Noack, «NO₂ Formation on the DOC/DPF System - a system thought,» in *AVL 6th International Exhaust Gas and Particulate Emissions Forum*, Ludwigsburg, 2010.
- [27] A. Winkler, D. Ferri e R. Hauert, «Influence of aging effects on the conversion efficiency of automotive exhaust gas catalysts,» *Catalysis Today* , n. 155, pp. 140-146, 2010.
- [28] A. Winkler, D. Ferri e M. Aguirre, «The influence of chemical and thermal aging on the catalytic activity of a monolithic diesel oxidation catalyst,» *Applied Catalysis B: Environmental*, n. 93, p. 77–184, 2009.
- [29] G. kostandopoulos, D. Zarvalis and I. Dolios, "Multi-Instrumental Assessment of Diesel Particulate Filters," 2007.
- [30] E. Wirojsakunchai, E. Schroeder, C. Kolodziej, D. Foster, N. Schmidt, T. Root, T. Kawai, T. Suga, T. Nevius e T. Kusaka, «Detailed Diesel Exhaust Particulate Characterization and Real-Time DPF Filtration Efficiency Measurements During PM Filling Process,» *SAE Technical Paper*, n. 2007-01-0320, 2007.
- [31] R. Montajir, T. Kusaka, I. Kaori, N. Kihara, I. Asano, M. Adachi e Q. Wei, «Soot Emission Behavior from Diverse Vehicles and Catalytic Technologies Measured by a Solid Particle Counting System,» *SAE Technical Paper*, n. 2007-01-0317, 2007.
- [32] Q. Salvat, P. Marez e G. Belot, «Passenger Car Serial Application of a Particulate Filter System on a Common Rail Direct Injection Diesel Engine,» *SAE Technical*

Paper, n. 2000-01-0473, 2000.

- [33] A. Konstandopoulos, D. Zarvalis, E. Papaioannou, N. Vlachos, G. Boretto, M. Pidria, P. Faraldi, O. Piacenza, P. Prenninger, T. Cartus, H. Schreier, W. Brandstätter, C. Wassermayr, G. Lepperhof, V. Scholz, B. Luers, J. Schnitzler, M. Claussen, A. Wollmann, M. Maly, G. Tsotridis, B. Vaglieco, S. Merola, D. Webster, D. Bergeal, C. Görsmann, H. Obernosterer, D. Fino, N. Russo, G. Saracco, V. Specchia, N. Moral, A. D'Anna, A. D'Alessio, R. Zahoransky, E. Laile, S. Schmidt e M. Ranalli, «The Diesel Exhaust Aftertreatment (DEXA) Cluster: A Systematic Approach to Diesel Particulate Emission Control in Europe,» *SAE Technical Paper*, n. 2004-01-0694, 2004.
- [34] M. Andreatta, F. Millo, F. Mallamo, C. Pozzi e D. Mercuri, «Experimental Investigation on Three Different Ceramic Substrate Materials for a Diesel Particulate Filter,» *SAE Technical Paper*, n. 2013-24-0160, 2013.
- [35] K. Tsuneyoshi e K. Yamamoto, «A study on the cell structure and the performances of wall-flow diesel particulate filter,» *Energy*, n. 48, pp. 492-499, 2012.
- [36] T. Mizutani, A. Kaneda, S. Ichikawa, Y. Miyairi, E. Ohara, A. Takahashi, K. Yuuki, H. Matsuda, H. Kurachi, T. Toyoshima, T. Ito, I. Lappas, C. D. Vogt, M. Tanaka, A. Martin, S. Fujii e P. Busch, «Filtration Behavior of Diesel Particulate Filters (2),» *SAE Technical Paper*, n. 2007-01-0923, 2007.
- [37] E. Jean e J. Michelin, «Improvement of the Compact Mixing Systems for Optimum SCR-Filter Integration on Passenger Cars,» in *23rd Aachen Colloquium Automobile and Engine Technology 2014*, Aachen, 2014.
- [38] M. Fischer, H. Kojima, T. Mito, N. Ohya, H. Haga, N. Sato e C. Beidl, «Efficiency Optimization of SCR Coated Particle Filters,» in *23rd Aachen Colloquium Automobile and Engine Technology 2014*, Aachen, 2014.

- [39] T. Wolff, R. Deinlein, H. Christensen e L. Larsen, «Dual Layer Coated High Porous SiC - A New Concept for SCR Integration into DPF,» n. 2014-01-1484, 2014.
- [40] R. Bonzi, L. Lietti, L. Castoldi and P. Forzatti, "NOx Removal Over a Double-Bed NSR-SCR Reactor Configuration," *Catalysis Today*, vol. 151, pp. 376-385, 2010.
- [41] F. Bunar, S. Schirmer, O. Friedrichs, C. Grünig, K. F. Hansen e J. Hartland, «High Performance Diesel NOx-Aftertreatment Concept for Future Worldwide Requirements,» in *23rd Aachen Colloquium Automobile and Engine Technology 2014*, Aachen, 2014.
- [42] A. Wereszczak, E. Fox, M. Lance e M. Ferber, «Failure Stress and Apparent Elastic Modulus of Diesel Particulate Filter Ceramics,» *SAE Technical Paper*, n. 2012-01-1252, 2012.
- [43] G. Merkel, D. Beall, D. Hickman e M. Vernacotola, «Effects of Microstructure and Cell Geometry on Performance,» *SAE Technical Paper*, n. 2001-01-0193, 2001.
- [44] k. Yuuki, «The Effect of SiC Properties on the Diesel Particulate Filter (DPF),» *SAE Technical Paper*, n. 2003-01-0383, 2003.
- [45] E. Ohara, Y. Mizuno, Y. Miyairi, T. Mizutani, K. Yuuki, Y. Noguchi, T. Hiramatsu, M. Makino, A. Takahashi, H. Sakai, M. Tanaka, A. Martin, S. Fujii, P. Busch, T. Toyoshima, T. Ito, I. Lappas e C. Vogt, «Filtration Behavior of Diesel Particulate Filters (1),» *SAE Technical Paper*, n. 2007-01-0921, 2007.
- [46] K. Ogyu, K. Ohno, S. Hong e T. Komori, «Ash Storage Capacity Enhancement of Diesel Particulate Filter,» *SAE Technical Paper*, n. 2004-01-0949, 2004.
- [47] S. Bensaid, D. L. Marchisio, N. Russo e D. Fino, «Experimental investigation of soot deposition in diesel particulate filters,» *Catalysis Today*, n. 147, 2009.

- [48] M. Lapuerta, J. Fernández e F. Oliva, «Effect of soot accumulation in a diesel particle filter on the combustion process and gaseous emissions,» *Energy*, vol. 47, pp. 543-552, 2012.
- [49] S. Miwa, F. Abe, T. Hammanaka, T. Yamada e Y. Miyari, «Diesel Particulate Filters Made of Newly Development SiC,» *SAE*, n. 2001-01-0192, 2001.
- [50] G. Merkel, W. Cutler e C. Warren, «Thermal Durability of Wall-Flow Ceramic Diesel Particulate Filters,» *SAE Technical Paper*, n. 2001-01-0190, 2001.
- [51] L. Kercher, D. Rose, T. Boger, W. Cutler, R. Dorenkamp, T. Düsterdiek e G. Kahmann, «Application of a New Filter Material in Volkswagen's Diesel Particulate Filter Systems,» Dresden, 2006.
- [52] C. Bischof, D. Rose, M. Ledger e M. Brogan, «Dura Trap AT Particulate Filters for Ford of Europe Passenger Cars with EU5 Emissions Legislation,» *Aachener Kolloquium Fahrzeug und Motortechnik*, 2009.
- [53] T. Boger, A. Joshua, J. Jamison, L. Warkins, A. Nancy, C. Warren e A. Heibel, «Next Generation Aluminium - Titanate Material to Meet Upcoming EU6 Emissions Legislation Requirments,» in *Aachener Kolloquium Fahrzeug und Motorentchnik 2010*, Aachen, 2010.
- [54] T. Boger, J. Jamison, J. Warkins e N. Golomb, «Next Generation Aluminum Titanate Filter for Light Duty Diesel Applications,» *SAE Technical Paper*, n. 2011-01-0816, 2011.
- [55] k. Iwasaki, «Innovative Aluminum Titanate Based - Diesel Particulate Filter Having Asymmetric Hexagonal Cell Geometry,» *SAE Technical Paper*, n. 2012-01-0838, 2012.

- [56] k. Nakamaura, N. Vlachos, A. Kostandopoulus e H. Iwata, «Performance Improvement of Diesel Particulate Filter by Layer Coating,» *SAE Technical Paper*, n. 2012-01-0842, 2012.
- [57] J. Seo, W. Park e M. Lee, «The Best Choice of Gasoline/Diesel Particulate Filter to Meet Future Particulate Matter Regulation,» *SAE Technical Paper*, n. 2012-01-1255, 2012.
- [58] J. Li e R. Mital, «Effect of DPF Design Parameters on Fuel Economy and Thermal Durability,» *SAE Technical Paper*, n. 2012-01-0847, 2012.
- [59] K. Yamamoto e K. Tsuneyoshi, «Experimental study of hexagonal and square diesel particulate filters under controlled and uncontrolled catalyzed regeneration,» *Energy*, n. 60, pp. 325 - 332, 2013.
- [60] F. Millo e D. Vezza, «Characterization of a New Advanced Diesel Oxidation Catalyst with Low Temperature NOx Storage Capability for LD Diesel,» *SAE Technical Paper*, n. 2012-01-0373, 2012.
- [61] e. a. Knafelz A., "Comparison of Diesel Oxidation Catalyst Performance on an Engine and a Gas Flow Reactor," *SAE paper 2007-01-0231*, 2007.
- [62] P. Carlsson, M. Skoglundh, P. Thorma e B. Anderssona, «Low-temperature CO Oxidation over a Pt/Al₂O₃ Monolith Catalyst Investigated by Step-response Experiments and Simulations,» *Topics in Catalysis*, Vol. 1 di 230-31, pp. 375-381.
- [63] K. Arnby, A. Törnqvist, B. Andersson e M. Skoglundh, «Investigation of Pt/γ Al₂O₃ Catalysts with Locally High Pt Concentrations for Oxidation of CO at Low Temperatures,» *Journal of Catalysis Volume*, vol. 221, n. 1, pp. 252-261, 2004.
- [64] S. Ye, Y. Yap, S. T. Kolaczkowski e K. Robinson, «Catalyst 'light-off' experiments on a diesel oxidation catalyst connected to a diesel engine—Methodology and techniques,»

Chemical Engineering Research and Design, vol. 90, n. 6, pp. 834-845, 2012.

- [65] Gamma Technologies Inc, in *GT-POWER User's Manual*, 2014.
- [66] T. Morel, R. Keribar e A. Leonard, «Virtual engine/powertrain/vehicle simulation,» *SAE Technical Paper*, n. 2003-01-0372, 2003.
- [67] F. Millo, M. Gianoglio Bernardi e P. Ferrero Giacominetto, «Analysis of different exhaust gas recirculation architectures for passenger car Diesel engines,» *Applied Energy*, n. 98, pp. 79-91, 2012.
- [68] M. André, «The ARTEMIS European driving cycles for measuring car pollutants emissions,» *Science of the Total Environment*, n. 334, pp. 73-84, 2004.
- [69] M. André, R. Joumard, R. Vidon, P. Tassel e P. Perret, «Real-world European driving cycles, for measuring pollutant emissions from high- and low-powered cars,» *Atmospheric Environment*, n. 40, p. 5944–5953, 2006.
- [70] E. Kladopoulou, S. Yang, J. Johnson, G. Parker e A. Konstandopoulos, «A Study Describing the Performance of Diesel Particulate Filters During Loading and Regeneration – A Lumped Parameter Model for Control Applications,» *SAE Technical Paper*, n. 2003-01-0842, 2003.
- [71] P. Flörchinger, U. Zink, W. Cutler e D. Tomazic, «DPF Regeneration-Concept to Avoid Uncontrolled Regeneration During Idle,» *SAE Technical Paper*, n. 2004-01-2657, 2004.
- [72] R. Zhan, Y. Huang e M. Khair, «Methodologies to Control DPF Uncontrolled Regenerations,» *SAE Technical Paper*, n. 2006-01-1090, 2006.
- [73] G. C. Koltsakis, O. A. Haralampous, Z. C. Samaras, L. Kraemer, F. Heimlich e K. Behnk, «Control Strategies for Peak Temperature Limitation in DPF Regeneration

Supported by Validated Modeling,» n. 2007-01-1127, 2007.

[74] P. Darcy, S. Guerry, G. Latouchent, P. Barbier e B. Fasolo, «Improvement of SiC DPF Control Strategies for Uncontrolled Regenerations with the Aid of Quasi 3D DPF Model,» *SAE Technical Paper*, n. 2008-01-1753, 2008.

[75] P. Recker e S. Pischinger, «Thermal Shock Protection for Diesel Particulate Filters,» n. 2011-01-2429, 2011.

List of Publications

[1] Andreato, M., Millo, F., Mallamo, F., Mercuri, D. et al., "Experimental Investigation on Three Different Ceramic Substrate Materials for a Diesel Particulate Filter," SAE Technical Paper 2013-24-0160, 2013, doi:10.4271/2013-24-0160.

[2] Andreato, M., Millo, F., Mercuri, D., Pozzi, C., Rafigh, M., " Impact on vehicle fuel economy of the soot loading on diesel particulate filters made of different substrate materials," Accepted on March 9, 2015. In press.